ABSTRACT

Title of dissertation: Modeling of Random Magnetization Dynamics in Nanosystems

Ziyu Liu, Doctor of Philosophy, 2014

Dissertation directed by: Professor Isaak Mayergoyz
Department of Electrical and Computer Engineering,
UMIACS and AppEl Center

Nonlinear magnetization dynamic process in nano-scale magnetic systems is of great scientific interests for its application to magnetic recording technology and spintronic devices. In the dynamic process, thermal fluctuation effects are of critical importance since they are directly related to long term reliability of magnetic devices. Recently, a novel approach to modeling stochastic magnetization dynamics has been proposed[1, 2, 3]. In this approach, thermal bath effects are accounted for by introducing a jump-noise torque term into the precessional magnetization dynamics equation. In this dissertation, we develop a Monte Carlo type numerical technique for implementation of the approach. There are two central elements of our numerical technique: a "midpoint" finite-difference scheme for integration of deterministic precessions and a "self-scattering" scheme which results in time-homogenization of a jump-noise process. The numerical technique unconditionally preserves the micromagnetic constraint and appreciably simplifies the random component of Monte Carlo simulations. We perform and illustrate numerous Monte

Carlo simulations in the dissertation using numerical examples. The Monte Carlo simulations are ideally suited for implementation on GPUs since they are intrinsically parallelizable in the sense that different realizations of stochastic magnetization dynamics can be computed concurrently. Therefore we develop a parallel algorithm and implement it using an Nvidia GPU card. A speed-up factor of more than 200 is achieved using this GPU implementation in comparison with the tranditional CPU single threaded implementation. Furthermore, we apply the jump-noise process driven magnetization dynamic equation to study random magnetization switching induced by thermal fluctuations. Numerical results demonstrate that the magnetization switching rate has a very different temperature dependence at relatively high and very low temperatures. The high temperature switching conforms to the Arrhenius law of thermal activation, whereas the low temperature switching has many features traditionally attributed to the phenomenon of macroscopic magnetization tunneling. The two temperature dependent regimes emerge directly from the properties of a jump-noise process while no quantum considerations are involved in our approach. Finally, we study the magnetization dynamics at elevated temperatures. We extend the jump-noise process driven magnetization dynamics approach and derive a generalization of the classical Landau-Lifshitz equation to describe magnetization dynamics around Curie temperature where the traditional micromagnetic constraint is not valid. The longitudinal and transverse damping terms in the generalized equation emerge directly from the mathematical structure of a jump-noise process which accounts for interactions with thermal bath.

Modeling of Random Magnetization Dynamics in Nanosystems

by

Ziyu Liu

Dissertation submitted to the Faculty of the Graduate School of the
University of Maryland, College Park in partial fulfillment
of the requirements for the degree of
Doctor of Philosophy
2014

Advisory Committee:
Professor Isaak Mayergoyz, Chair/Advisor
Professor Julius Goldhar
Professor Edo Waks
Professor Sennur Ulukus
Professor Howard Elman, Dean's Representative

Acknowledgments

I owe my gratitude to all the people who have made this thesis possible and because of whom my graduate experience has been invaluable and unforgettable.

First and foremost, I owe my deepest thanks to my parents. They have always stood by me and have pulled me through against impossible odds at times. Words cannot express the gratitude I owe them.

I would like to thank Professor Isaak Mayergoyz for all the valuable advice and guidance ever since I started to work on the research projects. He has superior knowledge on the magnetic materials and dynamics and has given me a lot of constructive suggestions and insights for my research. Without his positive support and generous help, this dissertation would be a distant dream.

I would also like to express my gratitude to Professor Julius Goldhar, Professor Edo Waks, Professor Sennur Ulukus and Professor Howard Elman for agreeing to serve on my thesis committee and for sparing their invaluable time attending my defense exam and reviewing this manuscript. I have benefited a lot from the ECE faculty team and I would like to thank all of them for the interesting classes, seminars and advice which help me think deeper about my research and career.

I would also like to thank my colleagues at the magnetics laboratory. They have offered generous help ever since I joined the group. Dr. Patrick McAvoy offered a lot of meaningful suggestions and helped me ordering and setting up the GPU used in the simulation. Andrew Lee coauthered several papers with me and we had very constructive and fruitful discussions. He also helped me by reviewing my writing.

Dr. Ling Hung, Dr. Garrett Lang and Dr. David Bowen have been very nice and helped me a lot in many ways. I have been very fortunate to know them in the way along my graduate studies.

Last but not least, I would like to thank all my friends for being emotionally supportive and bring me lots of good memories.

Table of Contents

List of Tables

List of Figures

Introduction

The study of magnetization dynamics in nano-scale magnetic materials has been the focus of considerable research for many years. This interest is driven by its theoretical importance as well as by its impact on the rapid development of scientific and engineering applications, including ferromagnetic resonances, hard disk drives and spin-torque nano-oscillators.

Magnetic recording is one of the most important examples of magnetic applications. The first idea of using magnetic materials for recording came out more than one hundred years ago when Oberlin Smith suggested in 1878 to use a silk or cotton thread impregnated with steel powder to record sound as a magnetic signal. This is exactly the idea on which modern magnetic recording is based. Over the next century, this idea was further developed. A audio tape cassette was successfully invented in 1963, and since then tape recorders became popular as consumer products[4]. The first magnetic hard drive was produced in 1956 when IBM created the IBM350 computer that incorporated a hard drive. This hard disk had a total capacity of 5 Mb consisting of 50 disks with an areal density of 2Kb per square inch. In the following sixty years, rapid development of computers has pushed the hard disk drives to achieve larger capacity, faster read/write speed, better stability and lower price. Nowadays, commercially available hard disk drives can store 3Tb or more and the areal density has increased to beyond 500Gb per square inch.

Figure 1 is a schematic illustruation of the principle of a magnetic hard disk drive. The recording medium is made of thin-film ferromagnetic materials. Ferromagnetic materials have spontaneous magnetization and the recording medium

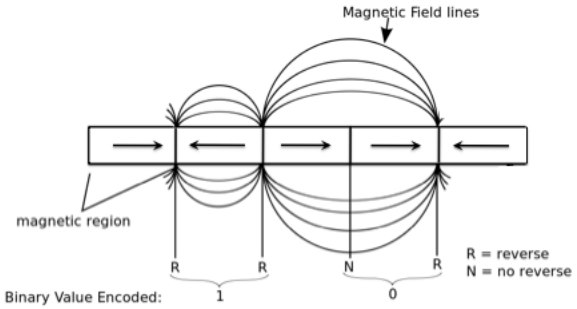

Figure 1: Schemtic structure of a hard disk drive

consists of a large number of small sized grains. In each grain the magnetization can have two distinguished stable states, where their orientations are antiparallel to each other. Due to this property, the orientation of the magnetization can be recorded as a bit of information. How the data is represented by the magnetic orientations is determined by the encoding scheme. Figure 1 shows a typical scheme to encode binary data where combinations of the directions of two neighboring grains can be coded to represent logical 0 and 1. This is the principle of data storage in a maganetic hard disk drive. The data can be rewritten and retrieved from the recording medium. Writing data to the recording medium is achieved through a writing head. During the writing process, voltage is applied to the head to induce current flows in the writing coil which generate a magnetic field at the gap and force the magnetization orientation at the magnetic bit to align with the magnetic field created at the gap. When the voltage is positive, the magnetic bit is polarized in one direction. When the voltage changes to negative, the magnetic field induced in the media also changes direction. The reading process utilizes a separate reading head. The reading head is a detector capable of converting magnetization orienta-

tions back to electrical signals. Currently the widely used reading head relies on the giant magneto-resistive (GMR) effect. The GMR effect was discovered in 1988 by Peter Gruenberg and Albert Fert, who won the 2007 Nobel Prize in Physics for this discovery. The GMR reading head is constituted by a multi-layers structure: two layers of ferromagnetic materials separated by a nonmagnetic metal spacer. One ferromagnetic layer is called the pinned layer which has a fixed magnetization and the other ferromagnetic layer is called free layer since its magnetization can change freely. Exchange interaction in magnetic materials tends to align nearby magnetization in the same direction. Consequently, when the head moves over the recording medium, the magnetization orientation in the free layer is influenced by the magnetic orientation of magnetized bit on the recording medium. Due to the GMR effect, change of the magnetization orientation in the free layer will induce a significant change in the electrical resistance of the multi-layers structure. When magnetization in the free layer and magnetization in the pinned layer are parallel, the electrical resistance is relatively low. Conversely, when they are antiparallel, the resistance is relatively high. Thus, by observing the electrical resistance of the GMR head, the information stored on the recording medium can be recognized.

One of the main challenges of magnetic storage devices nowadays is how to achieve higher recording density, faster read/write speed and better thermal reliability at lower costs. The recording density, speed and reliability are not independent issues and they are all related to the dynamic processes of magnetic materials. The areal density affects the reliability since a reduction in the size of the bit leads to a reduction in the energy barrier which separates the two magnetization states rep-

resenting logical 0 and 1 respectively. The height of the energy barrier determines the thermal stability of the written information. As the space required by a bit of information in a magnetic storage device shrinks, the effects induced by thermal fluctuations become increasingly important. When the energy barrier is comparable to the thermal energy, the magnetization becomes unstable and the inversion of the magnetization by thermal fluctuations is likely to occur. This effect is known as superparamagnetism and the corresponding limitation of the density is called superparamagnetic limit. Superparamagnetic effect can cause spontaneous switching of the magnetization, which modifies the stored data and results in data loss. Thermal fluctuations tend to destabilize the configuration of the magnetized bit. As a result, the smaller the size of the bit, the more likely a magnetization inversion will occur. In addition, as the areal density increases, the demand for higher write/read speed increases. Since the data writing speed is limited by the magnetization switching time, it is crucial to understand the magnetization dynamic processes for the optimal design of magnetic recording media. In this vein, my dissertation helps understand the time evolution of magnetic properties in magnetic particles and the magnetization reversal mechanism under various conditions, which shed light on the fundamentals of magnetic materials and the magnetization dynamic process.

Magnetic recording technology has been developing rapidly and several new designs have been invented recently. One such technology is the perpendicular recording. Originally the hard disk drive designs implemented longitudinal recording, where the magnetized bits were oriented horizontally and in-plane of the thin-film magnetic disk. More recently, a new perpendicular recording design has been incor-

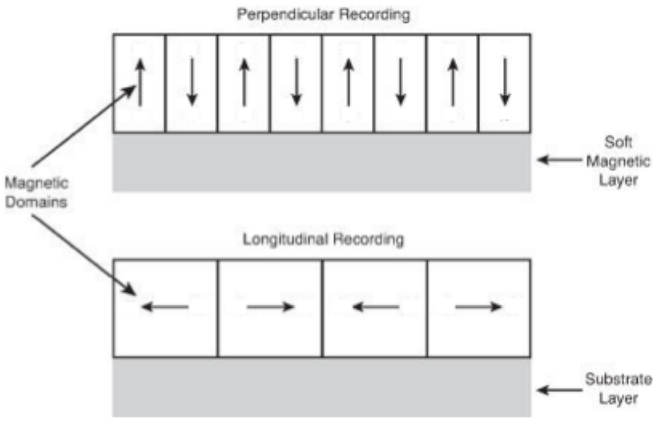

Figure 2: Recording medium structure of longitudinal recording and perpendicular recording

porated which aligns the magnetized bits vertically. This vertical design allows for closer magnetic domain spacing thus can achieve higher areal density than longitudinal recording. However, decreasing the size of a bit beyond the superparamagnetic limit could affect the reliability of the data stored. As pointed out earlier, when bit sizes are very small, superparamagnetic effect causes magnetization orientation to be unstable under the influence of temperature. Figure 2 shows schematically the difference between both recording solutions. The first commercially available hard disk drive using perpendicular recording was fabricated by Toshiba in 2005. It stores 40 GB on a single 1.8-inch platter and the areal density of this drive is 133Gb per square inch[5]. Another new technology of magnetic storage devices has being recently developed to enable future magnetic storage densities of up to 1000 Gb per square inch or more. This new approach is heat-assisted magnetic recording (HAMR). In the perpendicular recording the area to store a single bit is limited by

the superparamagnetic effect. To store data reliably for very small bit sizes, the magnetic medium must be made of a material with a very high coercivity, such as iron platinum alloy. However, since the bit size is very small and the coercivity is very high, the magnetic field used for writing data itself may not be strong enough to reverse the magnetization orientation so it can not write data to the disk. This difficulty can be overcome by raising the temperature of the magnetic medium where data is stored. This is achieved by applying an ultrafast pulsed laser locally to the magnetic grain so that the temperature at that region can go up to very close to the Curie temperature. In this way, the coercivity of the magnetic storage medium at the bit is lowered and a realistically achievable magnetic write field can be used to write data to the medium[6]. Understanding the magnetization dynamic processes in these techniques will greatly help optimizing the designs.

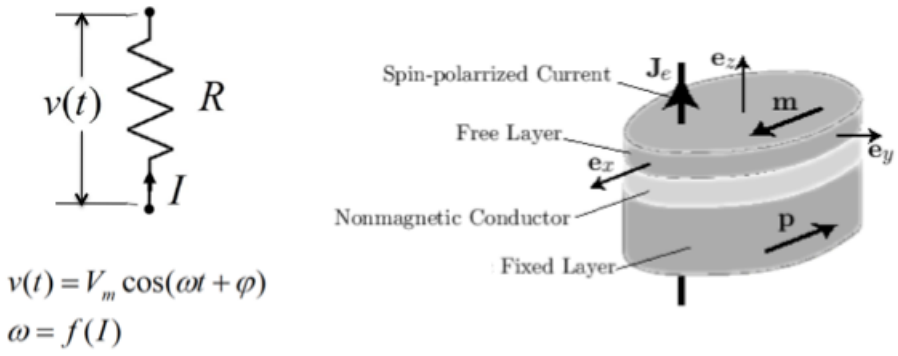

Figure 3: Schemtic illustration of spin torque nano oscillator

Besides novel designs of magnetic storage devices, another interesting phenomenon being discovered recently is the spin torque driven magnetization dynamics. Traditionally a direct current can only induce a constant voltage since the

electrical resistance has a relatively constant value. A nano-sized device has been developed so that a direct current can induce an oscillating voltage. The oscillation frequency is several gigahertz and can be tuned by the intensity of the current. This device is called spin torque nano oscillator (STNO)[7]. The design of the STNO is based on two spintronic effects: the spin torque and giant magneto-resistance effect. STNO has a multi-layers structure: there are two layers of ferromagnetic material separated by a nonmagnetic metal spacer. The incoming current is spin polarized by a first ferromagnetic layer which is the pinned layer. After flowing through a nonmagnetic spacer, the spin polarized current reaches the second ferromagnetic layer which is the free layer. The spin polarized current can induce the magnetization in the free layer to precess with frequencies in gigahertz range. The gigahertz oscillation of the magnetization can be detected as an AC voltage due to the giant magneto-resistance effects of the structure. The device resistance varies as the cosine of the angle formed by the magnetization vectors of two ferromagnetic layers varies, and as a result the output voltage varies. This phenomenon opens a new field known as spintronics. It is of great scientific interests to investigate spintronic effects since spintronic devices may potentially substitute the semiconductor devices in the future.

In addition to being applied to data recording and spintronic devices, nano-scale magnetic materials have improved the performance of many other applications such as sensors and actuators. More recently, the nano-scale magnetic materials are increasingly being used in applications in the life sciences and medicine techniques. For example, the magnetic nanoparticles can be used for cell labeling and drug

delivery[8].

To conclude, nano-scale magnetic structures have various scientifically interesting and technologically important properties. Therefore, the understanding of nanostructures and the study of their magnetic properties are of extreme significance. Whereas experiment on magnetic materials is a good way to understand their properties, a quantitative modeling of magnetic properties in nanostructured materials is also necessary to study magnetic technology. Theoretical analyses and numerical modeling of magnetization dynamics properties can help understand the magnetization dynamics mechanisms at extremely short or long timescales or at extremely low temperatures, which are normally experimentally not accessible. For example, experimental studies have difficulty in controlling magnetic properties down to the nanometer scale or close to absolute zero or a few kelvins in temperature[9]. Modeling of the dynamics processes on these scales poses no such problem. Magnetization dynamics modeling can deal with problems ranging from short timescale nonthermal precessional motions in nanoseconds to long timescale thermal stability up to years. It is of great interest to develop appropriate thermal and dissipative mechanisms and numerical models which could allow evaluation of the magnetization dynamics at both timescales. Since the spatial scale of magnetic recording media is in the order of hundred nanometers, magnetic properties of recording devices have to be analyzed by theoretical models with appropriate resolution. Moreover, the fast development of computational ability of computer processors in the last decade makes it possible to model complicated magnetic systems in acceptable time.

Microagnetic theory deals specifically with the behavior of magnetic materials

at sub-micrometer length scales. This theory started with a paper by Landau and Lifshitz in 1935[10] on the structure of the domain wall between two antiparallel magnetic domains. William Fuller Brown Jr. contributed several works on antiparallel domain wall structures around 1940[11, 12, 13] and gave this theory the name micromagnetics and used it as the title of his book in 1963[14]. In his book [14], Brown used a continuous magnetization vector to describe the transition region between magnetic domains instead of taking account of individual atomic moments as Landau did in [10]. The micromagnetic theory neglects the microscopic details by explaining magnetic properties and magnetization dynamic mechanisms at an intermediate length scale between magnetic domains and crystal lattice sites[15] and assuming that the magnitude of the magnetization vector for each point inside a magnetic structure is preserved.

In chapter one, the micromagnetic theory and magnetic interactions within magnetic systems are introduced. Then the micromagnetic model and the classical magnetization dynamics equations are discribed in details. Landau-Lifshitz[10] and Landau-Lifshitz -Gilbert[16, 17] equations are the most widely used equations for description of magnetization dynamics. Dynamics described by these equations contains precessional motion and transverse damping motion. The Landau-Lifshitz and Landau-Lifshitz-Gilbert equations are mathematically equivalent to each other and they are consistent with micromagnetic constraints. The constraints hold valid unless the temperature of the magnetic system goes very close to the Curie temperature. At elevated temperatures, Landau-Lifshitz-Bloch equation[18] can be used as an alternative to describe magnetization dynamics. The Landau-Lifshitz-Bloch

equation is a macroscopic equation for a ferromagnet at elevated temperatures and contains both transverse and longitudinal relaxation terms. It interpolates between the Landau-Lifshitz equation at relatively low temperatures and the Bloch equation at very high temperatures close to the Curie point. Thermal fluctuations are of great scientific importance since they are one of the dominant causes of intrinsic writing errors in magnetic data storage devices, and the stability of the information stored is of critical importance particularly as bits are made smaller and media are made thinner. The traditional approach to modelling magnetization dynamics in presence of thermal bath effects is presented in chapter one where a white-noise torque term is added to the classical Landau-Lifshitz or Landau-Lifshitz-Gilbert equation to account for the thermal effects. This approach was developed by Brown[19] in 1963 and has been widely used since then in modeling magnetization dynamics with thermal fluctuations. Recently, a different approach has been proposed[1, 2, 3] in which the thermal bath effects are accounted for by using a jump-noise torque term in the precessional magnetization dynamics equation. In this chapter it will be shown that this approach has clear advantages over the traditional one and both the damping and the fluctuation effects emerge from a single random process term: the jump-noise process.

In chapter two, we develop a numerical technique for this approach. The numerical technique has two central elements: a "mid-point" finite-difference scheme and a "self-scattering" technique. The mid-point finite-difference scheme is for numerical integration of deterministic precessional magnetization dynamics. Due to the mathematical structure of the mid-point finite-difference scheme, it uncondi-

tionally preserves the micromagnetic constraints in numerical simulations. This is a unique feature of the mid-point finite-difference scheme, since other numerical methods for differential equations pay little attention to the preservation of the micromagnetic constraints and the conservation of magnetization magnitude may be corrupted in the long run. The second central element of the numerical technique is the self-scattering technique used to determine the random scattering events. Instead of evaluating the scattering time using a complicated integral equation, an additional random scattering process is introduced into the dynamic equation and it results in zero jump of magnetization. Introduction of the "self-scattering" events leads to a time-homogenization of the jump-noise process, as a result, this technique appreciably simplifies the random component of Monte Carlo simulations. Then a Monte Carlo simulation of random magnetization dynamics driven by a jump-noise process is presented and some examples of Monte Carlo simulations are given to demonstrate the accuracy and efficiency of the numerical technique[20].

A main drawback of the CPU-based Monte Carlo simulation is the extensive computational burden. In chapter three, we develop a parallel algorithm to speed up the Monte Carlo simulations of magnetization dynamics driven by a jump-noise process by utilizing the computational power of general purpose Graphics Processing Units (GPUs). GPUs were originally developed for computer graphical processing but now they have been widely used for scientific computation because of its enormous parallel computational power. The Monte Carlo simulations are ideally suited for implementation on GPUs since they are intrinsically parallelizable in the sense that different realizations of stochastic magnetization dynamics can be computed

concurrently and independently. In our GPU implementation, there are two kernel functions executed on the GPUs. The first kernel function is used to precompute the scattering rate in parallel for ten thousand mesh points uniformly distributed over the sphere. The second kernel function is used to concurrently compute 10752 separate realizations of random magnetization dynamics. The accuracy and efficiency of this implementation are illustrated through simulations of thermal relaxations in uniaxial cobalt nanoparticles to the superparamagnetic state. To compare CPU and GPU speed, the code developed for the GPU implementation is carefully converted to a CPU equivalent code to perform exactly the same computations as the GPU code. A speed-up factor of about 200 has been observed in GPU Monte Carlo simulations in comparison with traditional single-threaded CPU simulations[21].

In chapter four, we apply the Landau-Lifshitz equation driven by a jump-noise process to study magnetization dynamics for a very wide range of temperatures. First, we investigate the random magnetization reversals in magnetic materials. For long timescale analysis, thermal decay of magnetization occurs due to thermal fluctuations which make it possible for magnetization to overcome the energy barrier and reverse its orientation in magnetic systems. This probability is normally given by Arrhenius' law. It has been demonstrated through experimental work[22, 23, 24] that there exists macroscopic tunneling effect of magnetization. At sufficiently low temperatures, macroscopic tunneling of magnetization causes the relaxation from one state to another to be enhanced above the thermally activated rate given by the classical Arrhenius' law. We derive a thermal switching model from the jump-noise driven magnetization dynamic equation, and numerical implementation of this

model shows consistency with the experimental observations described above. The high temperature switching agrees with the Arrhenius law of thermal activation, while the low temperature switching has many features traditionally attributed to the phenomena of macroscopic magnetization tunneling. And the two different temperature regimes are controlled by the thermal fluctuation through the parameters of the jump-noise process. Our derivation uses only the Kramers-Brown quasi-local equilibrium approximation without any additional assumptions, and the two temperature dependent regimes emerge directly from the properties of a jump-noise process while no quantum considerations are involved[25]. On the other hand, when the temperature of the magnetic systems is very close to the Curie temperature, the magnitude of magnetization is not conserved. Since both of the classical Landau-Lifshitz and Landau-Lifshitz-Gilbert equations are consistent with the micromagnetic constraint, they are not applicable for magnetization dynamics at elevated temperatures. For this reason, a generalization of the classical Landau-Lifshitz equation for the case of magnetization dynamics at elevated temperatures has to be investigated. A widely used model to describe magnetization dynamics at elevated temperature is the Landau-Lifshitz-Bloch[18] equation which is derived from the Fokker-Planck equation and the derivation uses the mean-field approximation. It is very desirable to develop one such generalization without approximations. We derive such a generalization based on the approach of describing the thermal bath effects by a jump-noise process, and the generalized equation coincides with the Landau-Lifshitz equation at low temperatures and is also valid when the temperature is very close to the Curie temperature. This equation has both longitudinal and

transverse damping terms, and the mathematical form of this equation is similar to the Landau-Lifshitz-Bloch equation. The uniqueness of our approach is that the longitudinal and transverse damping terms of our generalized equation emerge directly from the structure of a jump-noise process which accounts for thermal interactions, which is consistent with the physical origin of damping effects. The explicit formula of these parameters will be shown[26].

Conclusion is presented in chapter five and future research topics are introduced.

Results of this dissertation have been published in the following papers:

1. Z. Liu, A. Lee, G. Bertotti, C. Serpico, and I. Mayergoyz, *Jump-Noise Process Driven Magnetization Dynamics and Random Switching of Magnetization*, Journal of Applied Physics 111, 07D108 (2012).

2. A. Lee, Z. Liu, G. Bertotti, C. Serpico, and I. Mayergoyz, *Monte Carlo Simulations of Landau-Lifshitz Dynamics Driven by a Jump-Noise Process*, Journal of Applied Physics 111, 07D115 (2012).

3. I. Mayergoyz, G. Bertotti, C. Serpico, Z. Liu, and A. Lee, *Random Magnetization Dynamics at Elevated Temperatures*, Journal of Applied Physics 111, 07D501 (2012).

4. Z. Liu, A. Lee, P. McAvoy, G. Bertotti, C. Serpico and I. Mayergoyz, *Monte Carlo Simulations of Random Magnetization Dynamics on General Purpose Graphics Processing Units (GPUs)*, IEEE Transactions on Magnetics 49, 3133 (2013).

5. A. Lee, Z. Liu, G. Bertotti, C. Serpico, and I. Mayergoyz, *Analysis of random magnetization switching using Monte Carlo simulations*, to appear in Physica

B: Condensed Matter 2013.

6. G. Bertotti, C. Serpico, Z. Liu, A. Lee, and I. Mayergoyz, *Spin torque in the framework of random magnetization dynamics driven by a jump-noise process*, to appear in Physica B: Condensed Matter 2013.

Chapter 1

The Micromagnetic Model and the Dynamic Equations

To better understand the physics of the magnetization dynamics equations, we will start this chapter with a brief introduction of magnetization and its interactions that occur within ferromagnetic bodies at different spatial scales. The expressions of the energies related to each analyzed interaction are presented. Then the Brown's equations describing the equilibrium configurations are derived by imposing micromagnetic equilibrium as a 'stationary point' of the free energy. As a further step, a brief overview of the development of micromagnetic dynamic models is presented. Numerical modeling techniques related to micromagnetic dynamic models are also explained. Then thermal fluctuations are introduced into micromagnetic dynamic models because they are crucial for reliability of magnetic storage devices. The traditional approach to model magnetization dynamics in presence of thermal bath effects is discussed where a white-noise torque term is added to Landau-Lifshitz or Landau-Lifshitz-Gilbert equations to account for the thermal effects. A different approach has recently been proposed[1, 2, 3]. In this approach, the thermal bath effects are accounted for by using a jump-noise torque term in the precessional magnetization dynamics equation. At the end of this chapter it will be shown that this approach has clear advantages over the traditional one which uses a white-noise term to account for thermal bath effects.

1.1 Magnetization and Micromagnetic Interactions

Micromagnetics deals specifically with the behavior of magnetic materials at sub-micrometer length scales. This theory started with a paper by Landau and Lifshitz in 1935[10] on the structure of the domain wall between two antiparallel magnetic domains. William Fuller Brown Jr. contributed several works on antiparallel domain wall structures around 1940[11, 12, 13] and gave this theory the name micromagnetics in his book in 1963[14]. He emphasized that in this theory the microscopic details of the atomic structure were ignored and the material was considered from a macroscopic point of view by taking it to be continuous.

In micromagnetics, instead of describing the states of individual spins, the state of the ferromagnet is described by the magnetization $\mathbf{M} = \mathbf{M}(\mathbf{r}, t)$, which is the magnetic moment per unit volume. It is a function of position $\mathbf{r}$ and time t.

Micromagnetics is a continuum theory which means the magnetization can be regarded as a continuous function of space. When the temperature is well below the Curie temperature, the strong exchange interaction prevails over all other forces at the smallest spatial scale. Because of this continuum hypothesis, a fundamental constraint for micromagnetics is that at a given temperature that is well below the Curie temperature, the magnitude of magnetization at each point inside a ferromagnet is preserved and is equal to the spontaneous magnetization. This constraint can be expressed using the following equation:

$$|\mathbf{M}(\mathbf{r}, t)| = \mathbf{M}_s. \tag{1.1}$$

Micromagnetics deals with magnetic interactions arisen in a wide spatial scale,

going from few nanometers to few microns. In this respect, the micromagnetic framework includes short-range exchange and anisotropy interactions and long-range magnetostatic interactions between magnetic moments. All of these interactions can be described in terms of the micromagnetic free energy g. The micromagnetic free energy depends on applied field and temperature and can be expressed by the following volume integral[27]:

$$g(\mathbf{M}, \mathbf{H}_{\mathrm{a}}) = \int_{\Omega} [\frac{A}{M_s^2}((\nabla M_x)^2+(\nabla M_y)^2+(\nabla M_z)^2)+f_{AN}(\mathbf{M})-\frac{\mu_0}{2}\mathbf{M}\cdot\mathbf{H}_M-\mu_0\mathbf{M}\cdot\mathbf{H}_a]dV. \tag{1.2}$$

where Ω is the region that the ferromagnet is occupying, M_s is the spontaneous magnetization,M_x, M_y and M_z are components of magnetization in the cartesian coordinates, $f_{AN}(\mathbf{M})$ is the anisotropy energy density, $\mathbf{H}_M$ is the demagnetizing field and $\mathbf{H}_a$ is the applied magnetic field.

The first term inside the integral represents the exchange energy. The exchange interaction deals with spin-spin interactions and it tends to align neighboring spins so that the exchange energy penalizes nonuniformities in the magnetization orientation. The constant A is called the exchange stiffness constant. It can be experimentally identified but it is also possible to be estimated using a theoretical approach[27].

The second term describes crystal anisotropy effects where certain energy-favored directions exist for a given material. In the absence of an external field, the anisotropy effect makes the magnetization tend to be aligned along the easy direction. In a ferromagnet, the easy directions correspond to the minima of the anisotropy energy density $f_{AN}(\mathbf{M})$, whereas saddle-points and maxima of $f_{AN}(\mathbf{M})$

determine the medium-hard directions and the hard directions respectively.

The third term represents magnetostatic energy. The magnetostatic contribution is governed by the field $\mathbf{H}_M$, which is determined by solving the following magnetostatic Maxwell's equations:

$$\nabla \times \mathbf{H}_M = 0, \nabla \cdot \mathbf{H}_M = -\nabla \cdot \mathbf{M}, \tag{1.3}$$

using appropriate interface conditions at the ferromagnetic surface.

The last term is the energy due to the interaction with the external applied magnetic field $\mathbf{H}_a$. This energy term is also referred to in literature as the Zeeman energy.

The micromagnetic free energy may contain additional terms describing other energy contributions, for example magnetoelastic effects. These additional terms can be added to model when necessary.

1.2 Micromagnetic Equilibrium

From equation(1.2) we can calculate the free energy, if the magnetization distribution within the magnetic system is known. For constant external field and temperature, the micromagnetic equilibria are given by the minima of the free energy g. In order to find the energy extrema, a variation method has been proposed by Brown in his book *Micromagnetics*[14]. This variation method expresses the free energy variation δg corresponding to an arbitrary magnetization variation $\delta\mathbf{M}(\mathbf{r})$ subject to the constraint (1.1). The expression of the free energy variation is:

$$\delta g(\mathbf{M}, \mathbf{H}_\mathrm{a}) = -\mu_0[\int_\Omega \mathbf{H}_\mathrm{eff} \cdot \delta\mathbf{M} dV - \frac{2A}{\mu_0 M_s^2} \oint_\Sigma \frac{\partial \mathbf{M}}{\partial n} \cdot \delta\mathbf{M} dS], \tag{1.4}$$

where the effective field is defined as a sum of applied field, demagnetizing field, anisotropy field and exchange field:

$$\mathbf{H}_{\text{eff}} = \mathbf{H}_a + \mathbf{H}_M + \mathbf{H}_{AN} + \mathbf{H}_{EX}, \tag{1.5}$$

Here $\mathbf{H}_{AN}$ is the anisotropy field derived from the anisotropy energy:

$$\mathbf{H}_{AN} = -\frac{1}{\mu_0}\frac{\partial f_{AN}}{\partial \mathbf{M}}, \tag{1.6}$$

and $\mathbf{H}_{EX}$ is the exchange field defined as:

$$\mathbf{H}_{EX} = \frac{2A}{\mu_0 M_s^2}\nabla \mathbf{M}. \tag{1.7}$$

The effective field also identifies the direction of steepest energy decrease and can be calculated by means of

$$\mathbf{H}_{\text{eff}} = -\frac{1}{\mu_0 V}\nabla_\Sigma g. \tag{1.8}$$

By taking into account that at equilibrium, $\delta g = 0$ for any arbitrary $\delta\mathbf{M}$ consistent with (1.1), the following equations can be derived that at each point in Ω,

$$\mathbf{M} \times \mathbf{H}_{\text{eff}} = 0, \tag{1.9}$$

In other words, in equilibrium the magnetization is parallel to an effective field and the torque on the magnetization vanishes. This equation is known as Brown's equation. Using this equation the equilibrium configurations can be found for any magnetized body without describing how the magnetization reaches equilibrium during this time. And when using Brown's equation to find the equilibrium configurations, it is necessary to check if the solution is for a energy minimum or a energy maximum, for which situation the variation of energy vanishes too.

1.3 From Statics to Dynamics

The solution of Brown's equations gives us the magnetization distribution in equilibrium. However, real life magnetic systems are hardly ever in equilibrium. Usually the observed phenomena are time dependent, or, even if they are stationary, the systems are open due to the exchange of energy or another physical quantity. When $\mathbf{M} \times \mathbf{H}_{\text{eff}} \neq 0$, the system is not at equilibrium. In order to properly describe the evolution of the system, dynamic equations are introduced. The most commonly used deterministic dynamic equations are the Landau-Lifshitz equation proposed by Landau and Lifshitz in 1935 and the Landau-Lifshitz-Gilbert equation which is based on the Landau-Lifshitz equation and modified by Gilbert in 1955. It has been demonstrated that the Landau-Lifshitz-Gilbert equation is mathematically equivalent to the classical Landau-Lifshitz equation.

1.3.1 Landau-Lifshitz Equation

The Landau-Lifshitz equation is a dynamic constitutive relation that is compatible with micromagnetic constraints (1.1) and compatible with Brown's equation (1.9) at equilibrium. Namely, these constraints are the conservation in time of magnetization magnitude and the alignment of magnetization with the effective magnetic field at equilibrium. The Landau-Lifshitz equation is commonly written in the following form:

$$\frac{d\mathbf{M}}{dt} = -\gamma_L \mathbf{M} \times \mathbf{H}_{\text{eff}} - \alpha_L \mathbf{M} \times (\mathbf{M} \times \mathbf{H}_{\text{eff}}). \tag{1.10}$$

The dynamics described by the Landau-Lifshitz equation consists of two mo-

tions: precessional motion and damping motion. The first term on the right side corresponds to the precessional motion where γ_L is gyromagnetic ratio and determines the precession rate. The precessional motion can be derived from precessions of angular momentum of a electron. The magnetization precesses around the magnetic field direction and never reaches the equilibrium position unless it already points in the same direction. The precessional term is a conservative term in the sense that the precessional motion conserves both the magnetic moment magnitude and the free energy. It is known from experimental results that changes in the magnetization decay in finite time. So Landau proposed the damping term in the form of the second term on the right side. However, this damping cannot be derived rigorously from basic principles, it is just added by a phenomenological term. The phenomenological term represents only transverse relaxation since the magnitude of the magnetization is conserved. This term forces the magnetization rotates towards the direction of the effective field and eventually becomes parallel to it, reaching the equilibrium that is a stable state with a minimum of free energy. Parameter α_L is the damping constant which determines the damping rate. This part conserves the magnitude of magnetization but not the free energy of the system. Thus the equation as a whole is dissipative and does not conserve the energy, albeit conserving the magnitude of the magnetization.

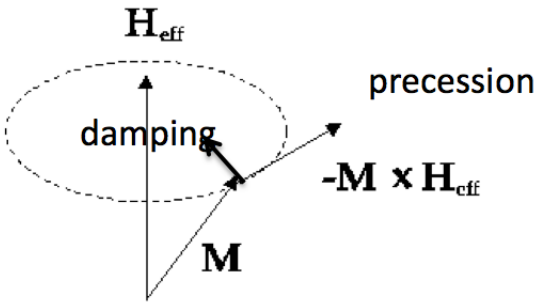

Figure 1.1: Damped precession motion of magnetization according to Landau-Lifshitz equation

1.3.2 Landau-Lifshitz-Gilbert Equation

Another equation typically used for the description of magnetization dynamics was proposed by Gilbert. This equation has the following form:

$$\frac{d\mathbf{M}}{dt} = -\gamma_G(\mathbf{M} \times \mathbf{H}_{\text{eff}}) + \frac{\alpha}{M_s}\mathbf{M} \times \frac{\partial \mathbf{M}}{\partial t}. \tag{1.11}$$

The Landau-Lifshitz-Gilbert equation is different from the Landau-Lifshitz equation in the definition of the damping component. The Gilbert damping term depends on the time derivative of the magnetic field. Similar to the Landau-Lifshitz equation, the Landau-Lifshitz-Gilbert equation preserves the magnetization magnitude.

The Landau-Lifshitz and the Landau-Lifshitz-Gilbert equations are the two most widely used equations for the description of the damped magnetization motion and they deal only with transverse relaxation. Such a transverse relaxation model is valid since the magnitude of magnetization of ferromagnet is conserved as long as the temperature is not too close to the Curie temperature. In addition, it can be demonstrated that t1he Landau-Lifshitz and the Landau-Lifshitz-Gilbert equations

are mathematically equivalent to each other[27]. The Gilbert version is typically preferred because the damping parameter can be assumed to be proportional to the intensity of the energy dissipation processes. This gives more physically reasonable results in terms of the dependence of the relaxation time on the damping parameter such that it predicts slower motion with increasing damping, whereas for the Landau-Lifshitz form it is true only for small damping[28].

1.3.3 Numerical Techniques

In recent years there has been a lot of work regarding the existence and regularity of solutions to the Landau-Lifshitz and Landau-Lifshitz-Gilbert equations[29, 30, 31, 32, 33, 34, 35, 36, 37, 38]. The Landau-Lifshitz and Landau-Lifshitz-Gilbert equations are highly nonlinear and analytical solutions to them exist only for some special cases. To understand the dynamic process described by this equation, a lot of attention has been put on numerical modeling of Landau-Lifshitz and Landau-Lifshitz-Gilbert equations.

Typically, the dynamic problem is first discretized in space by using finite difference or finite element methods[15]. This process reduces the problem to a ordinary differential equation. The resulting system requires at least a second order numerical scheme to obtain correct solution and the Heun method and Runge-Kutta method are the most widely used schemes[39]. Solving magnetization dynamics requires us to evaluate the energy term(1.2) which is a number of sums. The computational effort for n magnetic moments scales as n^2 as a result of the demagnetizing energy

term. Various techniques have been developed to attack this challenge. These include the direct FFT approach[40], the fast multiple method[41], the hybrid finite elements and boundary elements method[42], the Ewald summation approach[43] and the fast Fourier transfrom on multipoles method[44, 45].

There are several software packages available for simulations of the Landau-Lifshitz equation. They are the Object Oriented MicroMagnetic Framework (OOMMF) [46, 47] provided by the National Institute of Standards and Technology, Magpar [61, 62, 48] developed by Werner Scholz and the group of Prof. Fidler and Prof. Schrefl of the Technische Universitat Wien, Nmag [49] developed by Hans Fangohr, Thomas Fischbacher and Matteo Franchin from University of Southampton, and MuMax [50, 51] by Arne Vansteenkiste and DyNaMat group from Ghent University.

1.3.4 Landau-Lifshitz-Bloch Equation

There is an increasing need for higher areal density of magnetic data storage in hard disk drives. However, in current technology the area to store a single bit is limited by the superparamagnetic effect. For very small bit sizes, superparamagnetic effect causes magnetization randomly flip direction under the influence of thermal fluctuations. To store data reliably for very small bit sizes, the magnetic medium must be made of a material with a very high coercivity, such as iron platinum alloy. The only problem with the design is that since the bit size is very small and the coercivity is very high, the magnetic field used for writing data itself is not strong

enough to reverse the magnetization orientation and data can not be written to the disk. This problem can be solved by raising the temperature very close the Curie temperature so the coercivity of the magnetic storage medium at the bit is lowered and a realistically achievable magnetic write field can be used to write data to the medium. Currently, a laser is used to heat the material temporarily and locally. This technology is named heat-assisted magnetic recording (HAMR) by Seagate, where the name temperature-assisted recording(TAR) is used by Hitachi.

The classical Landau-Lifshitz and Landau-Lifshitz-Gilbert equations are consistent with the micromagnetic constraint and ignore longitudinal relaxation of magnetization dynamics. This restriction is true when the system temperature is well below the Curie temperature. However, magnetization dynamics in heat-assisted magnetic recording involves magnetization dynamics with temperature likely moving very close the Curie point on nanosecond timescales so the classical Landau-Lifshitz or Landau-Lifshitz-Gilbert equation doesn't work. In this case, the Bloch equation may serve as an alternative to the Landau-Lifshitz and Landau-Lifshitz-Gilbert equations since the temperature of the system is so close to Curie temperature that the magnetization magnitude is no longer preserved.

The Bloch equation was introduced by Felix Bloch in 1946[52]. It a phenomenological equation used to describe nuclear magnetic resonance and it is written as follows:

$$\frac{d\mathbf{M}}{dt} = \gamma \mathbf{M} \times \mathbf{H}_0 + \mathbf{H}_1 + \frac{1}{\tau_{ss}} \mathbf{e}_0 \times (\mathbf{e}_0 \times \mathbf{M}) + \frac{\mathbf{e}_0}{\tau_{sl}} (M_0 - \mathbf{M} \cdot \mathbf{e}_0). \tag{1.12}$$

where $\mathbf{H}_0$ is a applied dc magnetic field, $\mathbf{H}_1$ is a applied time-harmonic magnetic

field, $\mathbf{e}_0$ is a unit vector along the applied dc magnetic field, and τ_{ss} and τ_{st} are relaxation time constants. It is clear from the equation that there are two independent relaxation terms, one is parallel to the applied field and the other is perpendicular to it. The relaxation term parallel to the applied field is due to spin-lattice relaxation where the magnetization relaxes to the equilibrium saturation magnetization M_0 as a consequence of thermal fluctuation, while the relaxation term perpendicular to the applied field is attributed to spin-spin relaxation where phase coherence progressively disappear in the precession of the individual spins[27].

The Landau-Lifshitz-Bloch equation was derived by Garanin[18, 53] for both classical and quantum average spin polarizations. The Landau-Lifshitz-Bloch equation is a macroscopic equation for a ferromagnet at elevated temperatures and contains both transverse and longitudinal relaxation terms. It interpolates between Landau-Lifshitz equation at low temperatures and the Bloch equation at hightemperatures. In the derivation, the spin-bath interactions are described by stochastic Langevin fields and spin-spin interactions are treated within the mean-field approximation. With the assumption that external field changes slowly, the Landau-Lifshitz-Bloch equation is derived from the solution of Fokker-Planck equation. The equation has the following form:

$$\frac{d\mathbf{M}}{dt} = \gamma \mathbf{H}_{\text{eff}} \times \mathbf{M} + \frac{L_{\parallel}}{M_s^2}(\mathbf{M} \cdot \mathbf{H}_{\text{eff}})\mathbf{M} + \frac{L_{\perp}}{M_s^2}\mathbf{M} \times (\mathbf{M} \times \mathbf{H}_{\text{eff}}). \tag{1.13}$$

In this equation, the conservation of the magnetization magnitude is no longer a constraint. There are two independent relaxation mechanisms (transverse and longitudinal) for the magnetization components that are parallel and perpendicular

to the external field and $L_{\parallel}$ and $L_{\perp}$ are the longitudinal and transverse kinetic coefficients. It is valid beyond the Curie temperature while it coincides with the classical Landau-Lifshitz equation at low temperatures. Many simulations have been developed based on the Landau-Lifshitz-Bloch to model magnetization dynamics near Curie temperatures[54, 55, 56, 57, 58, 59].

1.4 Thermal Perturbations

The classical Landau-Lifshitz and Landau-Lifshitz-Gilbert equations describe magnetization dynamics at zero kelvin. At nonzero temperature, magnetization dynamics will be randomly perturbed by thermal fluctuations. Magnetic storage devices are usually very small such that the influence of thermal fluctuations can not be neglected. They will lead to random walks in a energy landscape and may eventually induce the magnetization to overcome the energy barrier and transition from one state to another. For this reason, thermal fluctuation is a dominant cause of error in magnetic storage devices and this process has been the subject of much study recently[15, 19, 27]. We will focus our study in this dissertation on magnetization dynamics in the presence of thermal fluctuations.

1.4.1 Stochastic Processes

The traditional approach to model thermal fluctuations is to add a white-noise process term to the classical Landau-Lifshitz or Landau-Lifshitz-Gilbert equation[19, 27, 60]. This approach was first developed by Brown in 1963. The assumption that

the thermal noise follows a Gaussian distributions is usually due to the central limit theorem. This is because the random fluctuations are the result of a very large number of statistically independent random fluctuation events, so the sum of these effects tends to have a Gaussian distribution.

In order to understand white-noise process, I will briefly review the Wiener process. The Wiener process is a continuous-time stochastic process and it is also called Brownian motion after the botanist Robert Brown.

The Wiener process $\mathbf{W}(t)$ is a zero mean Gaussian random process and is characterized by three properties,

1. $\mathbf{W}(t)$ satisfies the initial condition: $\mathbf{W}(0) = 0$.

2. $\mathbf{W}(t) - \mathbf{W}(s)$ is a Gaussian random variable with zero mean and variance $t - s$: $E[(\mathbf{W}(t) - \mathbf{W}(s))^2] = |t - s|$.

3. $\mathbf{W}(t)$ has uncorrelated increments: $E[(\mathbf{W}(t) - \mathbf{W}(t'))(\mathbf{W}(s) - \mathbf{W}(s'))] = 0$, if $[s', s]$ and $[t', t]$ are nonoverlapping intervals.

Though the Wiener process is not differentiable, a generalized derivative exists. And this generalized derivative of Wiener process is called Gaussian white-noise process. It is defined as follows:

$$\mathbf{h}_{\mathrm{N}}(t) = \frac{d\mathbf{W}(t)}{dt}. \tag{1.14}$$

The Gaussian white-noise is uncorrelated, independent, and can be charaterized by the following properties:

1. $E[\mathbf{h}_{\mathrm{N}}(t)] = 0$.

2. $E[\mathbf{h}_{\mathrm{N}}(t)\mathbf{h}_{\mathrm{N}}(s)] = \delta(t - s)$.

1.4.2 Stochastic Magnetization Dynamics

In the presence of thermal agitation, magnetization dynamics is usually studied by introducing appropriate stochastic terms in the Landau-Lifshitz or Landau-Lifshitz-Gilbert equation to account for the thermal fluctuation effects on the system. As discussed above, traditionally the stochastic term added to the Landau-Lifshitz or Landau-Lifshitz-Gilbert equation is a white-noise process term[19, 27, 60]. And this process is most commonly treated as a random component of the effective magnetic field and added to the dynamics equation as follows[19]:

$$\frac{d\mathbf{M}}{dt} = -\gamma\mathbf{M} \times (\mathbf{H}_{\text{eff}} + \nu\mathbf{h}_{\text{N}}(t)) - \frac{\gamma\alpha}{M_s}\mathbf{M} \times [\mathbf{M} \times (\mathbf{H}_{\text{eff}} + \nu\mathbf{h}_{\text{N}}(t))]. \tag{1.15}$$

where $\mathbf{H}_{\text{eff}}$ is the deterministic effective field which includes anisotropy, exchange, magnetostatic and external field interactions, ν is a parameter which controls the intensity of thermal perturbations. This parameter can be determined by the fluctuation-dissipation theorem[19, 65]

$$\nu^2 = \frac{2\alpha k_B T}{\mu_0 M_s^2 V}. \tag{1.16}$$

From the above equation, we can see that the intensity of thermal perturbations and the damping rate are related to each other. This is consistent with the physical nature of damping and thermal fluctuation since these two phenomena both results from the same interaction of the magnetization with the environment. However, the fluctuation-dissipation theorem relies on the assumption that the response of a system in thermodynamic equilibrium to a small applied force is the same as its response to a spontaneous fluctuation[27]. The fluctuation-dissipation theorem is

only valid for the stochastic magnetization dynamics in the vicinity of equilibrium. The fluctuation-dissipation theorem is no longer valid when the system is forced out of equilibrium by the presence of additional interactions such as the application of magnetic fields or the injection of electric currents.

By considering mathematical properties of Wiener process, the following Stochastic Landau-Lifshitz can be derived:

$$d\mathbf{M} = -\gamma[\mathbf{M} \times \mathbf{H}_{\text{eff}} + \frac{\alpha}{M_s}\mathbf{M} \times (\mathbf{M} \times \mathbf{H}_{\text{eff}})]dt + \nu\mathbf{M} \times d\mathbf{W}(t), \tag{1.17}$$

Equation (1.17) is a stochastic differential equation which has a drift (deterministic) and diffusion (noise) terms. The random magnetization dynamic process can be understood by solving this stochastic differential equation. There are two dominating versions of stochastic calculus, the Ito stochastic calculus and the Stratonovich stochastic calculus. The Ito integral is the usual choice in applied mathematics while the Stratonovich integral is frequently used in physics. An expression can be conveniently converted from an Ito form to an equivalent Stratonovich form, and vice versa. However, this stochastic equation (1.17) must be understood in the Stratonovich sense in this case. When it is interpreted in the Ito sense, the magnitude of magnetization is not preserved, ever worse, it blows up in finite time. A detailed derivation can be found in chapter 10 of *Nonlinear Magnetization Dynamics in Nanosystems*[27].

A more generalized form of magnetization dynamics with white-noise term is the stochastic LLB equation:

$$\frac{d\mathbf{M}}{dt} = \gamma \mathbf{H}_{\text{eff}} \times \mathbf{M} + \frac{L_{\parallel}}{M_s^2}(\mathbf{M} \cdot (\mathbf{H}_{\text{eff}}) + \nu \mathbf{h}_{\text{N}\parallel})\mathbf{M} + \frac{L_{\perp}}{M_s^2}\mathbf{M} \times (\mathbf{M} \times (\mathbf{H}_{\text{eff}} + \nu \mathbf{h}_{\text{N}\perp})). \quad (1.18)$$

This equation is valid even when thermal effects cause the temperature of the system to increase very close to the Curie temperature.

1.4.3 Numerical Techniques

Numerical simulations of stochastic Landau-Lifshitz equation have been developed using different choices of stochastic calculus and numerical integration schemes.

The most straightforward method of solving a stochastic differential equation is the Euler-Maruyama method[63]. It is similar to the Euler method of the deterministic case and it is easy to implement. But this stochastic Euler method converges to the Ito interpretation[63] so it is not applicable for magnetization dynamics analysis. The Stratonovich sense solution can be obtained by using the Milstein method[63]. This method is also a first order scheme but a numerical technique of at least second order is required to obtain correct results of the Landau-Lifshitz equation so this method won't work either. The proper techniques to solve this equation are the stochastic Heun method [64] and stochastic Runge-Kutta method. They are compatible with the Stratonovich interpretation and are of at least second-order[63, 39].

1.5 Jump-Noise Process Driven Magnetization Dynamics

As discussed above, magnetization dynamics has traditionally been modeled by introducing a white-noise torque term into the Landau-Lifshitz equation. In this

white-noise term approach, two distinct terms must be included in the dynamic equation: a deterministic damping term of either Landau-Lifshitz or Gilbert form and a white-noise torque term. However, the thermal interaction is also responsible for the damping, since fluctuations and dissipation are related phenomena resulting from the same interaction of the magnetization with its environment. The reason that two distinct terms are required in equation(1.17) is that the white-noise process alone cannot fully and adequately describe the random thermal effects. This is because the expected value of a white-noise process is always zero. The common physical origin of these two terms is traditionally accounted for by imposing fluctuation-dissipation relations. The fluctuation-dissipation theorem is only valid for the stochastic Landau-Lifshitz dynamics in the vicinity of equilibrium but questionable when dealing with far-from-equilibrium magnetization dynamics[1]. In addition, this approach does not show any magnetization dependence of the damping parameter. For these reasons, it is desirable to develop an approach that can fully describe the thermal bath effects by a single random process.

Recently, such a novel approach has been developed[1, 2, 3]. In this approach, a jump-noise process is introduced in the magnetization dynamics equations to account for random thermal effects. In this section, this approach will be discussed. First the Landau-Lifshitz equation driven by a jump-noise process is presented. It will be shown that unlike the white-noise approach, the jump-noise term itself can describe the thermal fluctuations and the Landau-Lifshitz and Gilbert damping terms can be derived as averages of the jump-noise process. It will also be demonstrated that this approach is more consistent with the physical origin of damping

and scattering in the sense that both damping and fluctuation effects emerge from a single noise term.

1.5.1 Mathematical Model

In this approach, a jump-noise process is introduced to account for thermal fluctuations. The jump-noise process can be defined by the following formula

$$\mathbf{T}_r(t) = \sum_i \mathbf{m}_i \delta(t - t_i), \tag{1.19}$$

where $\mathbf{m}_i$ is the i^{th} random magnetization jumps which occurs at random time t_i. The statistical properties of the jump-noise process are isotropic and independent of the orientation of the current magnetization state.

The stochastic magnetization dynamics driven by the jump-noise process can be mathematically described by the following stochastic differential equation[1, 2, 3]

$$\frac{d\mathbf{M}}{dt} = -\gamma(\mathbf{M} \times \mathbf{H}_{\text{eff}}) + \mathbf{T}_r(t), \tag{1.20}$$

where the first term on the right hand side represents the precessional dynamics of magnetization and $\mathbf{T}_r(t)$ is the jump-noise process that accounts for the thermal bath effects.

From equation (1.20) and (1.19) we can see that the stochastic magnetization dynamics described by them consists of continuous magnetization precessions randomly interrupted by random jumps in magnetization. This approach consideres magnetization dyanmics at relatively low temperatures so the micromagnetic constraint should be satisfied. Consequently, due to the strong local exchange in-

teraction, the magnitude of magnetization is preserved:

$$|\mathbf{M}(t)| = M_s = const, \tag{1.21}$$

Therefore, magnetization dynamics happens only on the the sphere Σ defined by equation (1.21) so the random jump process defined in (1.19) must also be defined on the sphere.

In order to solve the dynamics equation (1.20), the jump-noise process $\mathbf{T}_r(t)$ must be known. To completely describe the random process $\mathbf{T}_r(t)$, statistics of $\mathbf{m}_i$ and t_i must be given. This can be accomplished by specifying the transition probability rate $S(\mathbf{M}_i^-, \mathbf{M}_i^+)$, where $\mathbf{M}_i^- = \mathbf{M}(t_i^-)$ is the magnetization immediately before a random jump (scattering) at time t_i and $\mathbf{M}_i^+ = \mathbf{M}_i + \mathbf{m}_i = \mathbf{M}(t_i^+)$ is the magnetization immediately after the random jump . To satisfy the dynamic constraint (1.21), the transition probability rate $S(\mathbf{M}_i^-, \mathbf{M}_i^+)$ is defined on the sphere Σ.

By using the physical meaning of the function $S(\mathbf{M}, \mathbf{M}')$, the scattering rate of the jump-noise process $\lambda(\mathbf{M}(t))$ can be defined as

$$\lambda(\mathbf{M}(t)) = \oint_{\Sigma} S(\mathbf{M}(t), \mathbf{M}') d\Sigma'. \tag{1.22}$$

with the integration being performed over all $\mathbf{M}'$ on the sphere $|\mathbf{M}(t)| = M_s$.

It is clear that $\lambda(\mathbf{M}(t))dt$ is the probability of a magnetization scattering from $\mathbf{M}(t)$ to any $\mathbf{M}'$ on the sphere Σ during the time interval $(t, t + dt)$. Assuming the i^{th} jump event occurs at time t_i, the statistics of t_i and $\mathbf{m}_i$ can be defined by the

following formulas, respectively:

$$Prob(t_{i+1} - t_i > \tau) = e^{-\int_{t_i}^{t_i+\tau} \lambda(\mathbf{M}(t))dt}, \tag{1.23}$$

$$\chi(\mathbf{m}_i|\mathbf{M}_i) = \frac{S(\mathbf{M}_i, \mathbf{M}_i + \mathbf{m}_i)}{\lambda(\mathbf{M}_i)}, \tag{1.24}$$

where $\chi(\mathbf{m}_i|\mathbf{M}_i)$ is the conditional probability density of $\mathbf{m}_i$.

It is apparent from formula (1.24) that $\chi(\mathbf{m}_i|\mathbf{M}_i)$ satisfies the normalization condition

$$\oint_{\Sigma} \chi(\mathbf{m}_i|\mathbf{M}_i) d\Sigma_{\mathbf{m}_i} = 1, \tag{1.25}$$

where the integration is performed over all $\mathbf{m}_i$ such that $|\mathbf{M}_i + \mathbf{m}_i| = M_s$.

Also, from the statistic expressions of t_i (1.23) and $\mathbf{m}_i$ (1.24), we can see that the random magnetization dynamics can be fully defined provided that the transition probability rate $S(\mathbf{M}, \mathbf{M}')$ is known. A physically reasonable expression for $S(\mathbf{M}, \mathbf{M}')$ has been be found by studying the stochastic magnetization dynamics defined by equation (1.20) on the level of transition probability density $w(\mathbf{M}, t; \mathbf{M}_0, t_0)$[1]. It can be shown[100] that $w(\mathbf{M}, t)$ is the solution of the following partial differential equation

$$\frac{\partial w}{\partial t} = -\gamma \mathrm{div}_{\Sigma}[(\mathbf{M} \times \nabla_{\Sigma} g)w] + \hat{C}(w), \tag{1.26}$$

where $\hat{C}(w)$ is the Boltzmann-type collision integral given by the formula

$$\hat{C}(w) = \oint_{\Sigma} [S(\mathbf{M}', \mathbf{M})w(\mathbf{M}', t) - S(\mathbf{M}, \mathbf{M}')w(\mathbf{M}, t)] d\Sigma'. \tag{1.27}$$

By considering the transition prabablity density at thermal equilibrium, the following relation is obtained:

$$S(\mathbf{M}', \mathbf{M})w(\mathbf{M}', t) = S(\mathbf{M}, \mathbf{M}')w(\mathbf{M}, t). \tag{1.28}$$

This is the "detailed balance" condition and this condition is quite natural from the physical point of view in that it expresses the scattering process from any $\mathbf{M}$ to $\mathbf{M}'$ are equilibrated by its reversed process.

By using the "detailed balance" condition and aking the first three terms in the Taylor expansion, the transition probability rate can be expressed in the following form:

$$S(\mathbf{M}, \mathbf{M}') = Ae^{-\frac{|\mathbf{M}-\mathbf{M}'|^2}{2\sigma^2}} e^{\frac{g(\mathbf{M})-g(\mathbf{M}')}{2kT}}, \tag{1.29}$$

where A and σ^2 characterize the strength of thermal bath effects.

Since the expression for the transition probability rate $S(\mathbf{M}, \mathbf{M}')$ has been derived, the random magnetization dynamics can be fully defined. In this way, magnetization dynamics can be fully solved using the jump-noise process driven Landau-Lifshitz equation (1.20).

1.5.2 Discussion

It has also been demonstrated that the jump-noise process driven Landau-Lifshitz equation approach is more consistent with the physical origin of damping and scattering than the original approach where thermal noise is accounted for using a white-noise term. It has been shown that both damping and fluctuation effects emerge from the jump-noise term and the damping term for magnetization can be extracted as average effects caused by the jump-noise process $\mathbf{T}_r(t)$[1, 2, 3].

The jump-noise process can be written in the following form:

$$\mathbf{T}_r(t) = E[\mathbf{T}_r(t)] + \mathbf{T}_r^{(0)}(t), \tag{1.30}$$

where $E[\mathbf{T}_r(t)]$ is the expected value of the process while $\mathbf{T}_r^{(0)}(t)$ accounts for fluctuations.

Under the assumption that the magnitude of the process $\mathbf{T}_r(t)$ is small since only small jumps $\mathbf{m}(t)$ have non-negligible probability to occur, the following formula can be reached:

$$\mathbf{M}(t) \cdot E[\mathbf{T}_r(t)] \simeq 0. \tag{1.31}$$

This means that the expected value $E[\mathbf{T}_r(t)]$ is in the plane perpendicular to $\mathbf{M}(t)$. By choosing the basis vectors in this plane to be $\mathbf{M} \times \mathbf{H}_{\text{eff}}$ and $\mathbf{M} \times (\mathbf{M} \times \mathbf{H}_{\text{eff}})$, it can be found that

$$E[\mathbf{T}_r(t)] \approx -\gamma_L'(\mathbf{M} \times \mathbf{H}_{\text{eff}}) - \alpha_L(\mathbf{M} \times (\mathbf{M} \times \mathbf{H}_{\text{eff}})). \tag{1.32}$$

By substituting formula (1.32) into formula (1.30) and then into equation (1.20), the following equation can be reached:

$$\frac{d\mathbf{M}}{dt} = -\tilde{\gamma}_L(\mathbf{M} \times \mathbf{H}_{\text{eff}}) - \alpha_L(\mathbf{M} \times (\mathbf{M} \times \mathbf{H}_{\text{eff}})) + \mathbf{T}_r^{(0)}(t), \tag{1.33}$$

where $\tilde{\gamma}_L = \gamma + \gamma_L'$. The equation (1.33) is the Landau-Lifshitz equation randomly perturbed by the fluctuation $\mathbf{T}_r^{(0)}(t)$. It is also apparent from formula (1.32) that the average action caused by random thermal effects as described by the jump-noise process will result in the Landau-Lifshitz damping and a slight change of the gyromagnetic ratio which determines the precession rate.

It is also clear from the derivation that the gyromagnetic ratio γ and the damping constant α can be found by evaluating the expected value of the jump-noise process and decomposing it in terms of appropriate basis vectors. Since the expression for the transition rate $S(\mathbf{M}, \mathbf{M}')$ has been derived, we can evalute $E[\mathbf{T}_r(t)]$ and find the Landau-Lifshitz damping term α_L. By using formulas (1.24) and (1.29), the expected value of the jump-noise process is

$$E[\mathbf{T}_r(t)] = A \int \mathbf{m} e^{-\frac{|\mathbf{M}-\mathbf{M}'|}{2\sigma^2}} e^{\frac{g(\mathbf{M})-g(\mathbf{M}')}{2kT}} d\Sigma. \tag{1.34}$$

By taking into account that $\mathbf{M}-\mathbf{M}' = \mathbf{m}$ and $g(\mathbf{M})-g(\mathbf{M}') \simeq -\mathbf{m}\cdot\nabla_\Sigma g$, the expected value of the jump-noise process can be written in the following Gaussian-type integral:

$$E[\mathbf{T}_r(t)] \simeq A \int \mathbf{m} e^{-(\frac{|\mathbf{m}|}{2\sigma^2} + \frac{\mathbf{m}\cdot\nabla_\Sigma g}{2kT})} d\Sigma. \tag{1.35}$$

Due to the smallness of σ^2, the last integration formula is performed only for small $\mathbf{m}$ in the plane tangential to the sphere Σ so that

$$E[\mathbf{T}_r(t)] = -\frac{\pi\sigma^4}{kT} A e^{\frac{1}{2}(\frac{\sigma|\nabla_\Sigma g|}{2kT})^2} \nabla_\Sigma g. \tag{1.36}$$

In a similar way, by using formula (1.29) in equation (1.22) we derive

$$\lambda(\mathbf{M}) = 2\pi\sigma^2 A e^{\frac{1}{2}(\frac{\sigma|\nabla_\Sigma g|}{2kT})^2} \nabla_\Sigma g. \tag{1.37}$$

By substituting formula (1.37) into (1.36) and taking into account that

$$\nabla_\Sigma g = \frac{\mu_0 V}{M_s^2} \mathbf{M} \times (\mathbf{M} \times \mathbf{H}_{\text{eff}}), \tag{1.38}$$

the following expression for the damping constant can be found

$$\alpha_L = \lambda(\mathbf{M}) \frac{\sigma^2 \mu_0 V}{2kTM_s^2}. \tag{1.39}$$

This formula clearly reveals that the damping rate α_L depends on properties of the jump-noise process as well as on $\mathbf{M}$.

Chapter 2

Monte Carlo Simulation of the Jump-Noise Process Driven Magnetization Dynamics

In the previous section, stochastic magnetization dynamics driven by a jump-noise process has been discussed as an alternative to the traditional approach where magnetization dynamics is driven by a white-noise process. This alternative approach has clear advantages since both the damping and the fluctuations effects of the thermal bath emerge directly from the mathematical structure of a jump-noise process. However, due to the nature of the nonlinear equation, there exists no general analytical solution to this problem. In order to understand the dynamics, efficient numerical techniques for this approach need to be developed. In this chapter, such techniques are developed and a Monte Carlo simulation of this approach will be discussed in details.

2.1 Numerical Simulation Techniques

Typically when solving a magnetization dynamics process numerically, the magnetic system is first discretized in space by using finite difference or finite element methods[15]. In this way the magnetic dynamic system is reduced to a problem discribed by a ordinary differential equation. An appropiate time-stepping techinique is then required to numerically integrate the resulting equation.

As shown in chapter one, the stochastic magnetization dynamics driven by the jump-noise process can be mathematically described by the following stochastic differential equation

$$\frac{d\mathbf{M}}{dt} = -\gamma(\mathbf{M} \times \mathbf{H}_{\text{eff}}) + \mathbf{T}_r(t), \tag{2.1}$$

It is clear from the above equation that the random magnetization dynamics described by it has two distinct components: deterministic precessions described by the cross product term and a stochastic scattering described by the jump-noise process $\mathbf{T}_r(t)$. Accordingly, a numerical technique for integration of random dynamics must have two distinct components: a numerical scheme for integration of precessional dynamics and a numerical realization of random scattering described by $\mathbf{T}_r(t)$[20]. For numerical integration of deterministic precessions, as shown in chapter one, a numerical scheme of at least a second order accuracy is required to obtain a correct solution. While the Heun method and Runge-Kutta method are widely used to solve ordinary differential equations, they pay little attention to the preservation of the micromagnetic constraints. By using these schemes to solve the precessional dynamics the conservation of magnetization magnitude may be corrupted. This problem can be solved by using "mid-point" finite-difference scheme. These schemes unconditionally preserve the magnetization magnitude and are of second-order accuracy. The other central element of this simulation is the self-scattering technique used to determine the random scattering events. Instead of evaluating the scattering time using complicated integration, a more efficient self-scattering scheme can be implemented in our simulation. This technique greatly

simplifies the calculation of random scatterings and results in a time-homogenization of the jump-noise process.

2.1.1 Midpoint Finite-Difference Scheme

The deterministic component of magnetization dynamics can be obtained by solving the following differential equation:

$$\frac{d\mathbf{M}}{dt} = -\gamma(\mathbf{M} \times \mathbf{H}_{\text{eff}}). \tag{2.2}$$

This differential equation can be solved numerically using finite difference methods. Since we are going to use the numerical schemes to study long term magnetization dynamic behavior, it is crucial to have a accurate numerical time integration technique. Particularly, a technique preserves the micromagnetic constraints. For this reason, the following mid-point finite difference scheme[66] is used to find numerical solutions to equation (2.2):

$$\frac{\mathbf{M}^{(n+1)} - \mathbf{M}^{(n)}}{\Delta t_n} = -\gamma \frac{\mathbf{M}^{(n+1)} + \mathbf{M}^{(n)}}{2} \times \mathbf{H}_{\text{eff}}^{(n+\frac{1}{2})}. \tag{2.3}$$

Here, a temporal mesh consisting of the sequence of time instants $t_1, t_2, \ldots t_n$ is introduced for integration of (2.2), and $\Delta t = t_{n+1} - t_n$. $\mathbf{M}^{(n)}$ is the magnetization $\mathbf{M}$ at t_n, while $\mathbf{H}_{\text{eff}}^{(n+\frac{1}{2})}$ is the effective magnetic field evaluated at $t_{n+\frac{1}{2}} = t_n + \Delta t/2$. By using the Adams extrapolation formula, the following expression for the field $\mathbf{H}_{\text{eff}}^{(n+\frac{1}{2})}$ can be derived[27]:

$$\mathbf{H}_{\text{eff}}^{(n+\frac{1}{2})} = \frac{3}{2}\mathbf{H}_{\text{eff}}^{(n)} - \frac{1}{2}\mathbf{H}_{\text{eff}}^{(n-1)}. \tag{2.4}$$

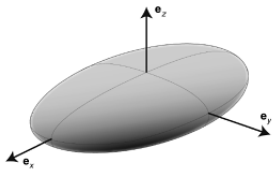

Figure 2.1: Ellipsoidal ferromagnet in the cartesian reference frame.

We can assume that the ferromagnetic nanoparticle is of ellipsoidal shape, and initial distribution of magnetization and parameters are spatially uniform. Under these conditions, the demagnetizing field is spatially uniform and can be expressed in terms of a demagnetizing tensor. We also assume that the nanoparticle has uniaxial anisotropy and the direction of the easy axis is aligned with one of the axes of the ellipsoid. In this case, the effective field can be expressed as:

$$\mathbf{H}_{\text{eff}} = (H_{ax} - D_x M_x)\mathbf{e}_x + (H_{ay} - D_y M_y)\mathbf{e}_y + (H_{az} - D_z M_z)\mathbf{e}_z, \tag{2.5}$$

where D_x,D_y,D_z are parameters that account for demagnetizing and crystal anisotropy effects, H_{ax}, H_{ay}, H_{az} are the components of $\mathbf{H}_a$ along $\mathbf{e}_x$, $\mathbf{e}_y$, $\mathbf{e}_z$. And the free energy is of the following form:

$$g(\mathbf{M}, \mathbf{H}_{\text{a}}) = [\frac{1}{2}(D_x M_x^2 + D_y M_y^2 + D_z M_z^2) - H_{ax} M_x - H_{ay} M_y - H_{az} M_z]\mu_0 V. \tag{2.6}$$

The mid-point finite difference scheme equation provides a second order of accuracy in time and it can be shown that it preserves the micromagnetic constraints unconditionally. Through the dot-multiplication of both sides of this equation by $\mathbf{M}^{(n+1)} + \mathbf{M}^{(n)}$, it can be obtained that

$$|\mathbf{M}^{(n+1)}|^2 = |\mathbf{M}^{(n)}|^2 = M_s^2. \tag{2.7}$$

This conservation of magnetization magnitude is valid for any form of the function $\mathbf{H}_{\text{eff}}^{n}$ used in the the mid-point finite difference scheme and any time step value. Furthermore, this property is valid for any excitation condition (constant or time-varying applied fields, constant or time-varying spin-transfer effects, various anisotropy properties, etc.)[27]. Thus, this mid-point finite difference scheme preserves the magnetization magnitude in numerical computations.

It also can be shown that in the case of constant applied field, the following energy balance relation can be derived:

$$\frac{g(\mathbf{M}^{(n+1)}) - g(\mathbf{M}^{(n)})}{\Delta t_n} = 0. \tag{2.8}$$

This confirms that the free energy is preserved using the mid-point finite-difference scheme regardless of the choise of $\mathbf{H}_{\text{eff}}^{n}$ or time steps.

Since the mid-point finite-difference scheme preserves exactly the magnitude and the microscopic free energy regardless of the time step, for the sake of simplicity, constant time steps are implemented in our simulation. The accuracy of this finite difference scheme can be judged by the "ability" of this scheme to preserve $g(\mathbf{M}^{(n)})$ in numerical computations. The value of $g(\mathbf{M}^{(n)})$ is proved numerically to be conserved for pressional motions described by this scheme. It is also clear that if the magnetic energy g is conserved in the computations, then the numerical precessional trajectory must be closed. And indeed, numerical integrations of precessional dynamics using the mid-point scheme with sufficiently small time-step Δt results in closed numerical precessional trajectories. This is illustrated by Figure 2.2 where examples of closed numerical precessional trajectories are presented.

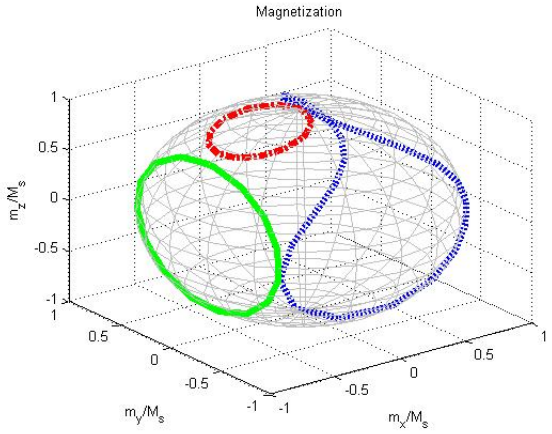

Figure 2.2: Closed precessional trajectories computed for different anisotropy settings and different values of applied fields ($D_x = 0.4132$ $D_y = 0.4132$ $D_z = 0.0946$ $H_{ax} = 0.2$ $H_{ay} = 0$ $H_{az} = 0$, $D_x = 0.4132$ $D_y = 0.4132$ $D_z = 0.0946$ $H_{ax} = -0.1$ $H_{ay} = 0$ $H_{az} = 0$, $D_x = 0.0946$ $D_y = 0.4132$ $D_z = 0.4132$ $H_{ax} = 0$ $H_{ay} = 0$ $H_{az} = 0$)

2.1.2 Self-Scattering Technique

After solving the precessional dynamics numerically, a numerical realization of random scattering described by $\mathbf{T}_r(t)$ need to be developed. In our approach, a self-scattering technique is developed to calculate the random component of magnetization dynamics. This techinique can greatly simplify the random component of the simulations, and is adopted from Monte Carlo simulations of semiclassical transport of electrons and holes in semiconductors[67, 68].

As shown in chapter one, the probability that a ferromagnet which scattered the time t_i has not yet experienced another scattering after a time τ is defined by the following formula:

$$Prob(t_{i+1} - t_i > \tau) = e^{-\int_{t_i}^{t_i+\tau} \lambda(\mathbf{M}(t))dt}. \tag{2.9}$$

This formula gives the probability of a scattering (jump) free precessional time

intervals $(t_i, t_i+\tau)$. Consequently, the probability that the magnetization will scatter during $d\tau$ around time τ can be given by

$$P(\tau)d\tau = \lambda(\mathbf{M}(\tau))e^{-\int_{t_i}^{t_i+\tau}\lambda(\mathbf{M}(t))dt}d\tau. \tag{2.10}$$

The scattering events should be selected stochastically in accordance with the statistics given by (2.10) in the simulation. However, since the scattering rate $\lambda(\mathbf{M}(t))$ is a function of $\mathbf{M}(t)$, we need to calculate and store the value of $\lambda(\mathbf{M}(t))$ at each time step along a magnetization trajectory and evaluate the integral equation at each time step to determine if a scattering event should happen. Due to the complexity of the integral at the exponent, it is not efficient to determine the scattering (jump) free precessional time intervals τ directly from (2.10). This is why the numerical realization of the random part is complicated. Simulations of charge transport in semiconductors have a very similar situation when dealing with the free flight duration and Rees has developed a method[69, 70] to overcome this difficulty. He introduced a new fictitious "self-scattering" such that the total scattering probability, including the self-scattering, is constant. This technique can be implemented here to simplify the simulation of scattering events in magnetization dynamics processes. This can be achieved by introducing an additional random scattering process $\mathbf{T}_r^{(0)}(t)$ which does not change the actual magnetization dynamics. In other words, instead of evaluating the actual scattering rate in (1.20) we numerically simulate the solution of equation

$$\frac{d\mathbf{M}}{dt} = -\gamma(\mathbf{M}\times\mathbf{H}_{\text{eff}}) + \mathbf{T}_r(t) + \mathbf{T}_r^{(0)}(t). \tag{2.11}$$

The random process $\mathbf{T}_r^{(0)}(t)$ is defined by the transition probability rate $S_0(\mathbf{M}_i, \mathbf{M}_{i+1})$

given by the following formula

$$S_0(\mathbf{M}_i, \mathbf{M}_{i+1}) = \lambda_0(\mathbf{M}_i)\delta(\mathbf{M}_{i+1} - \mathbf{M}_i). \tag{2.12}$$

By using the last formula and equation (1.24), we find

$$\chi_0(\mathbf{m}_i|\mathbf{M}_i) = \delta(\mathbf{m}_i), \tag{2.13}$$

which means that the random "scattering process $\mathbf{T}_r^{(0)}(t)$ results in zero jumps of magnetization. For this reason, this process is called self-scattering. This terminology is adopted from the area of Monte Carlo simulations of charge transport in semiconductors to calculate free flight duration[67, 68]. It is clear from (2.13) that the introduction of the self-scattering event does not affect the actual stochastic magnetization dynamics. However, by choosing an appropriate self-scattering rate we can achieve time-homogenization of the total $(\mathbf{T}_r(t) + \mathbf{T}_r^{(0)}(t))$ jump-noise process. In this way, the numerical calculation of jump time will be considerably simplified. The choice of $\lambda_0(\mathbf{M})$ should be in such a way that the total scattering rate Γ is constant as shown in the following formula:

$$\lambda(\mathbf{M}(t)) + \lambda_0(\mathbf{M}(t)) = \Gamma = const. \tag{2.14}$$

This is illustrated in Figure 2.3 where the relation between the real scattering rate, self-scattering rate and total scattering rate is shown.

The random duration τ of magnetization precession without scattering as define by (1.23) can be simplified using the total scattering process such that

$$Prob(t_{i+1} - t_i > \tau) = e^{-\Gamma\tau}. \tag{2.15}$$

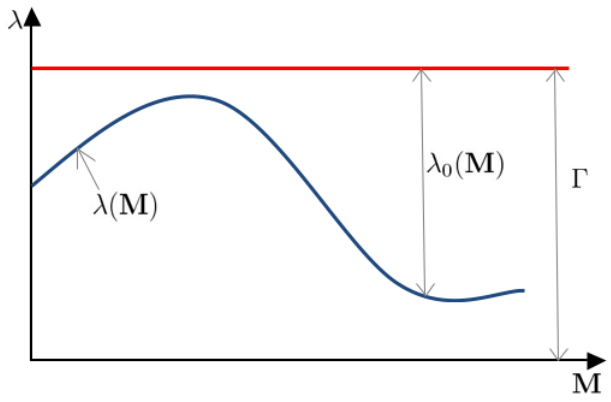

Figure 2.3: Definitions of actual scattering rate, self-scattering rate and total scattering rate in self-scattering technique ($D_x = 0.4132$ $D_y = 0.4132$ $D_z = 0.0946$ $H_{ax} = 0$ $H_{ay} = 0$ $H_{az} = 0$)

This equation implies that the probability $P(\tau)$ of scattering during the time interval τ does not depend on t_i and is given by the formula

$$P(t \leq \tau) = 1 - e^{-\Gamma\tau}. \tag{2.16}$$

From this equation, the random duration without scattering can be randomly generated each time from the probability distribution $P(\tau)$. An inverse transform sampling method is used to obtain the random intervals. This is a general method for generating random sample numbers x from any probability distribution given its cumulative distribution function $F(x)$[71, 72]. When the distribution function is simple enough that its inverse $F^{-1}(x)$ can be found, a random number x can be obtained from a uniformly distributed random number by

$$x = F^{-1}(r). \tag{2.17}$$

where r is a uniformly distributed random number between 0 and 1.

In our case, using formula (2.16) the random duration τ of magnetization

precession without scattering can be generated from the following formula:

$$\tau = -\frac{1}{\Gamma}\ln[1 - P(\tau)]. \tag{2.18}$$

Thus, by generating a random number P uniformly distributed between 0 and 1 and using the above formula, we can generate the random duration τ of magnetization precession and the random time $t_{i+1} = t_i + \tau$ at which the next scattering occurs. Since the self-scattering rate should not be negative, the total scattering rate is always greater than (sometimes equal to) the actual scattering rate. In this sense, the scattering events generated by (2.18) occur more frequently than the actual scattering events and the simulation wastes time in taking care of self-scattering events. However, the time "wasted" is far more than compensated for by the simplification of the calculation of the integral equation. For this reason, the "self-scattering" technique determines the timing of the scattering events far more efficiently than equation (2.10) does. The magnetization experiences only precessional dynamics till next scattering occurs. So the magnetization state $\mathbf{M}(t_{i+1}^-)$ before a scattering occurs can be found by integrating the precessional dynamics over the time interval τ using the mid-point finite-difference scheme.

After generating the random scattering time and the magnetization state right before the scattering occurs, we have to determine if the scattering at t_{i+1} is due to the actual jump-noise process defined by $S(\mathbf{M}, \mathbf{M}')$ and given by formula (1.23) or if it is a self-scattering event defined by $S_0(\mathbf{M}, \mathbf{M}')$ using (2.12). In order to determine the scattering mechanism, we need to know the actual scattering rate and total scattering rate at the time of scattering event. Since the probability density of

actual scattering and self-scattering at time t_{i+1} is proportional to $\lambda(\mathbf{M}(t_{i+1}^-))$ and $\lambda_0(\mathbf{M}(t_{i+1}^-))$ respectively, we can first generate a random number ν that is uniformly distributed between 0 and Γ . Then the discrimination between these two scattering events can be accomplished using the following rules: when comparing the value of ν and the actual scattering rate, if $0 < \nu < \lambda(\mathbf{M}(t_{i+1}^-))$, an actual scattering occurs at t_{i+1} and the magnetization after the scattering event $\mathbf{M}(t_{i+1}^+)$ can be determined using the conditional probability density specified by formula (1.24). Otherwise, if $\lambda(\mathbf{M}(t_{i+1}^-)) < \nu < \Gamma$, the actual scattering event does not occur and a self-scattering event is performed. That is, a self-scattering occurs at t_{i+1} and the magnetization does not change $\mathbf{M}(t_{i+1}^+) = \mathbf{M}(t_{i+1}^-)$. Then, by using formula (2.18), a new random time interval τ of precessional motion is generated and the steps described above are repeated.

The two central elements of our simulation are described above. The dynamics described by using the mid-point finite difference scheme and the self-scattering technique can be illustrated by Figure 2.4, which shows that the magnetization dynamics occurs on the sphere and consists of magnetization precessions randomly perturbed by jumps.

2.2 Monte Carlo Simulation

The evolution of an individual particle governed by random magnetization dynamics can be solved by the above numerical techniques. Because of the random nature of the jump-noise process, the magnetization dynamics solved by the above

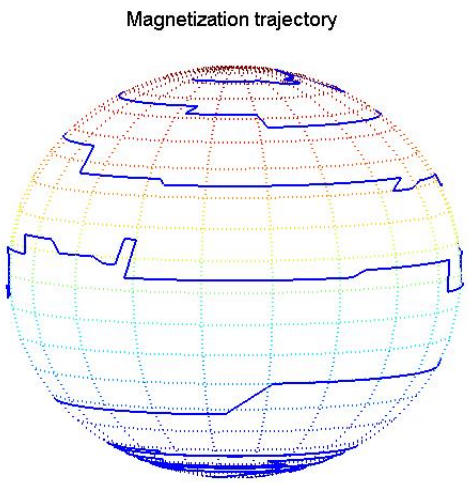

Figure 2.4: An example of magnetization dynamics trajectory

numerical teniques is random. The timing of the jumps and the jumps themselves are randomly determined by their probability distribution functions such that they have inherent uncertainty. As a result, the dynamics calculated based on these random jumps is just one of the possible realizations of the system. In order to better understand the time evolution of the system, it is appropiate to use the Monte Carlo method. By calculating the results over and over again using the same numerical techniques as mentioned above, but each time using different random values from the probability distribution functions, the Monte Carlo simulation can produce distributions of possible realizations. In this way, the Monte Carlo simulation gives a much more comprehensive way of describing uncertainty of the magnetization dynamics of a magnetic system and provides macroscopic properties of magnetization dynamics under thermal fluctuations. Not only can possible realizations be provided, but also how likely each realization would be to happen. Furthermore, our

simulation is intrinsically parallel in the sense that different realizations of random magnetization dynamics can be computed independently. Thus the Monte Carlo method is suitable for our problem.

Because of the random nature of Monte Carlo simulation, the results from each calculation may be different even when the number of realizations per calculation is the same. Thus it is important to know how many realizations we will have to calculate in order to safely assume that we have taken "enough" realizations and to see how accurate our Monte Carlo simulation result is, given a certain number of realizations. These two issues are related in the sense that the more accurate we want our result to be, the more realizations we need to take, and the more realizations we take, the more likely it will be that we will get a more accurate estimate. Unfortunately, it is not possible to achieve perfect accuracy through sampling unless we could sample the entire population of possible evolution trajectories of the system. What we implemented to ensure the accuracy of our simulation is to set the number of realizations in such a way that further doubling the number of calculations will not change the simulation result by more than 0.1 percent.

2.3 Numerical Results

To test the accuracy of the described numerical techniques, thermal relaxations of an uniaxial cobalt particle to the superparamagnetic state have been simulated.

We consider a ferromagnetic nanoparticle with uniaxial anisotropy. The direction of the easy axis is aligned with the z-axis of the ellipsoid. When there is no

applied field, the magnetization has two equilibrium states, one is along the z direction while the other is along the -z direction. In sufficiently small nanoparticles, the potential barrier created from the anisotropy would be insufficient to separate the two states when the fluctuations are strong enough. At this size, the rate at which the magnetization will randomly reverse direction becomes significant. The system becomes superparamagnetic. In the superparamagnetic state, the equilibrium distribution has the following Boltzmann-type form[19]

$$w^{eq}(\mathbf{M}) = \frac{1}{Z}\exp(-\frac{g}{kT}), \tag{2.19}$$

where Z is the normalization factor.

Specifically when there is no applied field, the equilibrium distribution has the following form:

$$w^{eq}(\mathbf{m}) = \frac{1}{Z(\mu)}\exp[-\frac{\mu}{2}(D_z m_z^2 + D_\perp(1-m_z^2))], \tag{2.20}$$

where

$$Z(\mu) = \oint_\Sigma \exp[-\frac{\mu}{2}(D_z m_z^2 + D_\perp(1-m_z^2))]d\Sigma. \tag{2.21}$$

In the last two formulas, $\mathbf{m}$ is the particle magnetization normalized by M_s, D_z and $D_\perp$ are anisotropy constants along the z-axis and in the plane perpendicular to this axis, while $\mu = \mu_0 M_s^2 V/kT$. The equilibrium distribution $w^{eq}(\mathbf{m})$ has been computed through Monte Carlo simulations. Comparisons between the Boltzmann expression and numerical simulations are presented in Figures 2.5 and 2.6 for different sets of anisotropy parameters specified in the figure captions. In both cases, the agreement between Monte Carlo simulations and the Boltzmann formula

is quite good. Figure 2.7 presents the plot of $m_z(t)$ for one specific realization of random magnetization dynamics. From the figure we can see that the random switching occurs very frequently in the superparamagnetic state.

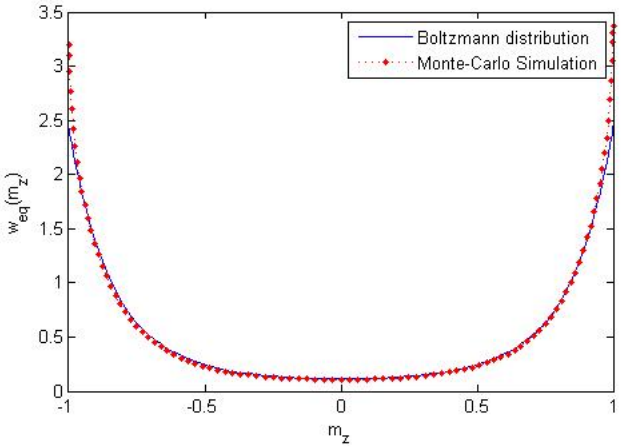

Figure 2.5: Equilibrium distribution in the superparamagnetic state of uniaxial cobalt nanoparticle (computations performed for the following parameters: $D_x = 0.4132$ $D_y = 0.4132$ $D_z = 0.0946$ $M_s = 1.42 \times 10^6$ $\gamma = 1.837$ $T = 300$ $V = 2 \times 10^{-25}$ $\sigma = 0.1$ $B = 10^{12}$)

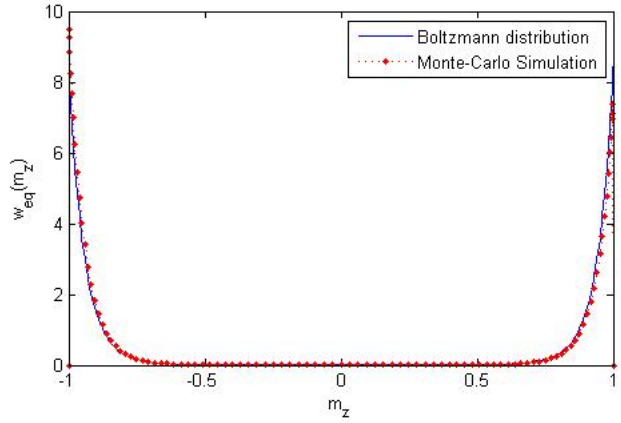

Figure 2.6: Equilibrium distribution in the superparamagnetic state of uniaxial cobalt nanoparticle (computations performed for the following parameters: $D_x = 0.49$ $D_y = 0.49$ $D_z = 0.02$ $M_s = 1.42 \times 10^6$ $\gamma = 1.837$ $T = 300$ $V = 2 \times 10^{-25}$ $\sigma = 0.1$ $B = 10^{12}$)

We also use this Monte Carlo simulation to show a time evolution of the prob-

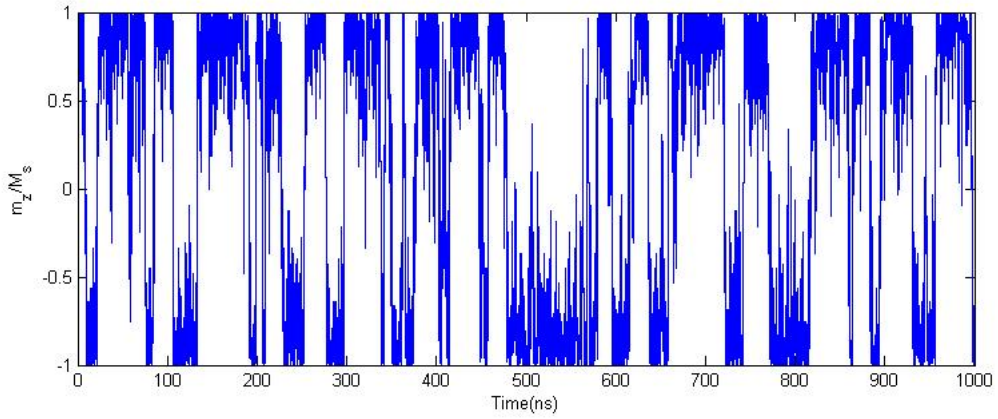

Figure 2.7: Plot of m_z over time

ability that magnetization is in one certain energy well of a system. The magnetization is initially at the equilibrium state in well one so at initial state the probability that magnetization is in well one is equal to one. The magnetization goes away from the equilibrium and experiences precessions and random jumps due to the thermal fluctuations. Since the energy barrier created from the anisotropy is not sufficient to separate the two states, the magnetization will randomly go beyond the barrier and reverse its direction. The probability that magnetization is in energy well one will eventually equal to the probability that magnetization is in energy well two when the particle reaches superparamagnetic state. And both of the probabilities will be 0.5. This is illustrated in figure 2.8. The curve is not perfectly smooth due to the fact that the Monte Carlo simulations are not able to sample all the possible realizations. We have also compared results from simulation implemented with self-scattering technique and simulation using the integral equation without the self-scattering technique. The time evolutions of the probability of two approaches are identical but the self-scattering technique saves a lot of computational time and

resources. From the above analysis of the calculation performance, the mid-point finite-difference and self-scattering numerical techniques are a reasonable choice for producing adequate results in an acceptable calculation time.

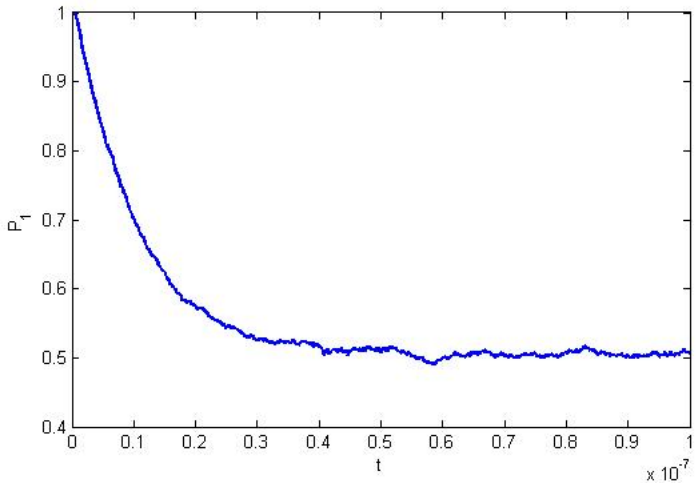

Figure 2.8: Plot of time evolution of the probability that magnetization is in one certain energy well

Chapter 3

Magnetization Dynamics Simulation on GPUs

In the previous chapter, Monte Carlo simulations of magnetization dynamics driven by a jump-noise process have been discussed. However, a main drawback of the CPU-based Monte Carlo simulation is the extensive computational burden. Some of our simulations of long-term magnetization dynamics require weeks of calculation on a CPU. In order to reduce simulation time, we utilize the parallel computation ability of GPUs to speed up our Monte-Carlo Simulation. The details of such a implementation will be described in this chapter.

Knowledge of computer architectures is helpful to understand difference between CPUs and GPUs and how to expedite different kinds of numerical calculations. Michael Flynn proposed a classification of computer architectures in 1966[74]. There are four classifications in Flynn's taxonomy, defined by the number of concurrent instructions and the number of data streams. They are single instruction single data (SISD), single instruction multiple data (SIMD), multiple Instruction single data (MISD) and multiple instruction multiple data (MIMD). SISD and MISD architectures process data sequentially so they are not of spectacularly interests in our simulation.

SIMD architecture refers to a parallel computer that runs the exact same program on each of its parallel units which contain different data. In SIMD processor,

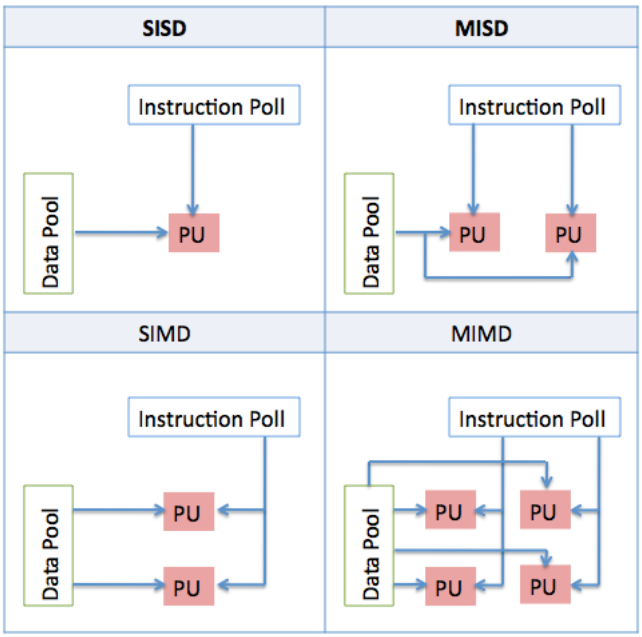

Figure 3.1: Principles of SISD, SIMD, MISD and MIMD systems

there is a global controller unit with many processors and all the processors do the same task. For the nature of this architecture, SIMD is used to perform operations which may be naturally parallelized. Since SIMD is relatively simple to design, it is less expensive.

MIMD architecture refers to a parallel computer that runs independently different instructions on each of its simultaneously-executing parallel units which contain different data. In MIMD, each processor is assigned an independent controller and each processor will be doing an independent task. Because of the complexity MIMD processors tend to be expensive, but it can solve very complex problems. Clusters and most of supercomputers are based on a MIMD architecture.

A GPU (Graphics Processing Unit) has a massively multi-threaded architecture. The multi-threaded architecture is designed to perform identical calculations

on different data sets which are the same idea as SIMD. This architecture is ideal for graphical processing which enables real-time rendering 3D graphics scenes in parallel in computer games. That was the reason why GPUs were originally developed. But now the GPUs have been widely used for scientific computation because of its enormous parallel computational power. Significant savings of computing time have been reported in micromagnetic modeling by implementing GPU computations in comparison to single CPU core implementations. For example, a micromagnetic simulator called GPMagnet is built recently and a speedup factor of two orders of magnitude is achieved[73], 1000 times speedup has been achieved to perform Monte Carlo simulations of photon migration[76], and 35 times speedup has been achieved for Ising model of the ferromagnetic phase transition[75]. There is also an increasing popularity of implementing simulation on GPUs in a lot of other scientific applications such as solving Kepler's equation[77], air pollution modeling[78], financial markets modeling[79], dose calculation[80], volume reconstruction from X-ray images[81], molecular dynamics simulations[82], and quantum chemistry[83].

GPU's highly parallel data structure makes it more effective than a general-purpose CPU for algorithms that have a large fraction of the computation done in parallel. From the previous chapter we can see that the Monte Carlo simulations are intrinsically parallelizable in the sense that different realizations of stochastic magnetization dynamics can be computed concurrently and independently from one another. For this reason, GPU is especially suited for our Monte Carlo simulations where a large number of different realizations of random magnetization dynamics are computed based on a series of identical arithmetic operations. When running Monte

Carlo simulations on a CPU using single-threaded implementation, simulations of random trajectories are computed one after another. As a result, the CPU-based Monte Carlo simulations are very time consuming. By taking advantage of GPUs, the same program can be executed on many data elements in parallel, thus the simulation is performed much faster. Also, GPUs are much less expensive than MIMD systems like clusters or supercomputers. For these reasons we choose to use GPUs for our Monte Carlo simulations.

We use an NVIDIA GTX 460 for the simulation, which has a Fermi architecture and is incorporated with 7 multiprocessors, 336 cores and offers 1GB GDDR5 global memory while costs about $180. This NVIDIA card is controlled by the host CPU-type computer which has two Intel Xeon processors at 2.13 GHz with 48 GB RAM. Our work is based on NVIDIA's Compute Unified Device Architecture (CUDA), a hardware and software architecture for general-purpose computing on graphics processing units (GPGPU) specifically designed for NVIDIA GPUs. CUDA programs are based on the C programming language with certain extensions to utilize the parallelism of the GPU.

3.1 GPU Architecture

In general, CPUs contain a few very powerful multiprocessors with up to a few cores each that can handle multi-threading. These cores are very powerful and fast but are still intrinsically sequential such that instructions are handled serially. This limits the processing speed when a large number of tasks can and should be

completed simultaneously. To handle this, CPU multiprocessors use complicated pipelining algorithms to switch between tasks and therefore requires large memory caches to hold data in storage while it waits to be processed.

Unlike CPUs, GPUs don't have sophisticated control logic and excessive memory caches but process a large number of arithmetic logic units (ALUs) for doing actual computations. GPUs differ from CPUs in that while each GPU multiprocessor is not very powerful on its own, there are a large number of multiprocessors optimized to provide very high floating point arithmetic for a same problem. In this way, the large number of computations that need to be completed can be distributed between the cores such that each core can work on the problem quickly and independently.

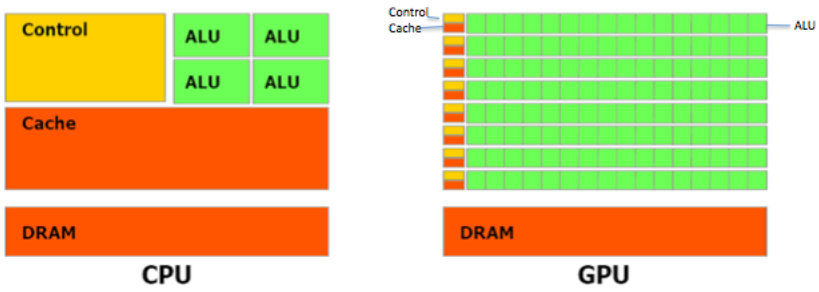

Figure 3.2: Architectural differences between CPUs and GPUs

When a kernel is called to be performed on GPUs, they will be executed N times in parallel. Each of these realizations is executed independently by a GPU "thread". To align with the physical hardware, these threads are grouped into "blocks", which themselves are grouped into a "grid". Threads can be grouped to form a one-dimensional, two-dimensional, or three-dimensional block, and blocks

can be grouped to form a one-dimensional, two-dimensional, or three-dimensional grid. This grouping structure provides a natural way to perform computations using vectors, matrixes, or volume elements[84]. We will utilize this grouping structure to distribute the Monte Carlo simulations onto the 336 cores of a NVIDIA GTX 460. An illustration of GPU thread hierarchy is shown in Fig 3.3[84].

Threads within a block are all processed on the same processor, can share data via fast shared memory and can coordinate their execution. Because of the limited memory resources of the core, there is a limit to the number of threads per block. For NVIDIA GTX 460, the maximum number of threads per block is 1024. The number of blocks in a grid is usually a multiple of the number of processors in the system and is dictated by the size of the data being processed. The total number of threads executed in parallel N, as defined above, is equal to the number of threads per block times the number of blocks[84]. The threads execute independently from one another, and even the execution order of the threads is not controllable. Thus a thread should never rely on the results from another parallel thread. GPUs are capable of switching rapidly between different threads, and this ability effectively hides memory latency when there are a large number of threads in a program. The ability of hiding memory latency ensures that the hardware is working on arithmatic calculations at all times rather than waiting for data to be trasfered so it largely improves GPU performance.

There are multiple memory spaces on the GPU that the threads can access during their execuation. Each thread has private local memory, access to which is extremely fast. Threads combined in a block have shared memory that can be ac-

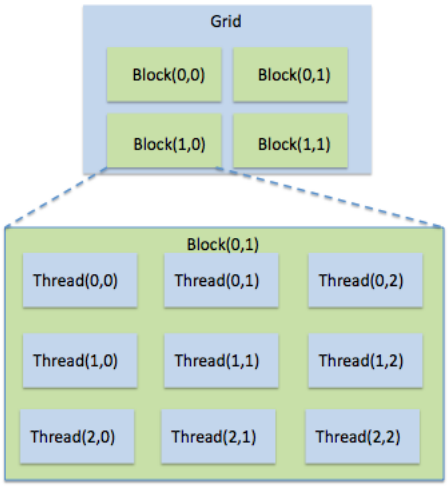

Figure 3.3: Schematic representation of GPU thread hierarchy[84]

cessed by all threads in that block. This memory can be accessed essentially without significant memory latency so it is normally used to synchronize and communicate between the threads in a block. There is also global memory that is accessible by all threads being executed, but accessing global memory in the middle of a kernel will cause a latency of several hundred clock cycles. There are also two additional read-only memory spaces accessible by all threads: the constant and texture memory spaces. The several layers of very high bandwidth memory also improve the GPU performance.

Several general steps should be taken to run GPU computations. First, any data required in the calculation should be copied from the host computer to the GPU memory. Then the CPU calls the process on the GPU, which is called a "kernel", and the GPU operates on the data. Next, the data is copied back to the host to use it in the rest of the program or so another "kernel" can be called to further process the data on the GPU.

3.2 GPU Implementation vs. CPU Implementation

In the CPU implementation of the Monte Carlo algorithm, a total scattering rate has to be generated before the random magnetization dynamics calculations. The total scattering rate (the lambda threshold), as defined in the self-scattering technique, is set to be a constant in each calculation to achieve time-homogenization of the scattering events. In most of our calculation we set the total scattering rate to be 1.2x the maximum value of the scattering rates at each point on the sphere. The scattering rates are magnetization orientation dependent and each of them have to perform a integration of transition probability density on the whole sphere, so the calculation of total scattering rate will be time consuming when we use a fine mesh. After calculating the total scattering rate, random jump times are first calculated along with the magnetization vector. The magnetization for the next time step is then calculated using the Mid-point Finite Difference Scheme based on the Landau-Lifshitz equation. If the current time is greater than the calculated random jump time, it means a random jump has occurred and random numbers are generated to determine if it is a self-scattering event or an actual scattering event and the new scattered magnetization if it is a real scattering event. Once this process is completed, the current time is incremented and the process repeats. This process occurs for each time step for each Monte Carlo trial and is very computationally intensive.

For the GPU implementation of the Monte Carlo algorithm, both the total scattering rate calculation and the realizations of random magnetization evolutions

are computed in parallel. The scattering rates at each point on the sphere can be calculated independently from each other so that they are computed in parallel on GPU. In addition, the fact that each Monte Carlo trial of the magnetization dynamics is independent lends itself very nicely to parallelization. In fact, the same process is followed as the CPU implementation with the exception of having each graphics processing core only handling one or a few Monte Carlo trials. This considerably speeds up the processing time.

3.2.1 Random Number Generator

A key component in our GPU implementation of the Monte Carlo simulations is the random number generators (RNGs) that provide the independent stochastic input to each realization. Our simulation requires a large number of realizations and each realization runs a large number of time steps. As a result, it is very important to have a random number generator that gives a long sequence of independent numbers that are indistinguishable from a true random number source for each thread in parallel and in a quick manner. A common way to generate pseudo-random numbers for Monte Carlo simulations is to use the same random number generator with different seed, such as a timestamp. However, when we are running many threads concurrently on GPUs this method will result in many threads performing exactly the same computations. One option would be to use the same random number generator but with a different seed for each thread. Moreover, in our case the number of parallel processes is large, the number of random numbers in each

process is large, so the total number of random numbers required is very large. Even the random number generator could be perfectly seeded, the period of a random number generator may not be long enough thus the simulation may end up using the same sequence of random numbers. Therefore there are two key properties a RNG should have to be used in our simulation: a long period and a good statistical quality.

One of the oldest and best-known RNGs is the linear congruential generator (LCG) [87], which uses a transition function of the form $x_{n+1} = (ax_n + c) mod$ m. If c = 0, the generator is often called a multiplicative congruential generator (MCG), or Lehmer RNG. If c 0, the method is called a mixed congruential generator. The maximum period of the generator is m, since GPUs run by 32-bit integer, the period can be at most 2^{32}, which is far too low. Another generator that is commonly used in Monte Carlo simulations is the lagged Fibonacci generator[87]. This generator is similar to an LCG but introduces a delayed feedback. However, to achieve good quality, the delayed feedback must be large. Consequentially a certain amount of memory must be used to hold the state for the delayed feedback. However, in the NVIDIA GPU architecture, the available memory per thread is limited. So a RNG that requires less memory is prefered. The Mersenne Twister[86] is also one of the most widely used methods for random number generation in software. It has a period of $2^{19937} - 1$ and a extremely good statistical quality. These properties make the Mersenne Twister a really good candidate for our RNG. However, it presents problems similar to those of the lagged Fibonacci, because it requires more than a thousand bytes of states that must be updated serially.

To solve this problem, we have employed a revised 4-cycle multiplicative congruential RNG[88]. This generator features a long period of about 2^{120} and good statistical quality. More importantly, this generator is easy to implement in code and it requires only 16 bytes of states which could be updated independently in each realization. Another beauty of this approach is that each individual thread could have a different seed so that they all generate unique sequences of random numbers while requiring a minimum amount of memory.

3.2.2 GPU Simulator

The simulator is built of two layers. The first layer is the main function which handles all simulation host tasks that are running on the CPU. This includes defining simulation parameters, generating the mesh, initializing magnetization and seeding the random number generators. It also allocates memory structures in the GPU memory and copies all the data needed for the simulation from the CPU memory to the GPU global memory.

When all of the data is copied, the CUDA kernel is called. This kernel function is the second layer of our simulator and is executed on the GPU. Our simulator has two distinct kernel functions. The first kernel function is called to precompute the scattering rate. These computations are performed in parallel for ten thousand mesh points uniformly distributed over the sphere. The results of these computations are arranged in a square matrix, which is copied to the CPU. These computations are used to find the maximum of the scattering rate, which is used in the choice of

self-scattering rate to guarantee the constant total scattering rate.

The second kernel function is called to concurrently compute different realizations of random magnetization dynamics. Each thread contains one Monte Carlo realization of the dynamics. In our simulations, 42 blocks of 256 threads have been concurrently executed. In this way, 10,752 separate realizations of random magnetization dynamics are simultaneously computed. As the numerical techniques used in CPU simulation discussed in Chapter two, the second kernel function here also has two distinct components: a numerical integration of deterministic precessional dynamics using the "mid-point" finite difference scheme and a numerical implementation of random magnetization scattering. It copies the data from global memory to the multiprocessor registers, performs a certain number of time steps for each thread and then copies the magnetization state at each time step back to global memory. After all threads are done, the data is copied back from the global memory and written to a output file. Though all threads execute the same programmable instructions, the computations of different realizations of magnetization dynamics are not synchronized in time. This is because random magnetization scatterings occur at different random times for different realizations.

Another thing to point out is that the second kernel function has to be called multiple times, performing a limited number of time steps each time. This is because the Windows Watchdog timer prohibits any program to use the GPU for more than approximately 5 seconds. Hence, the calculation has to be divided into smaller parts. This gives the program a chance to give updates to the user regarding the progress of the simulation. The downside of this solution is a slightly increased

simulation time. Since register memory only has the lifespan of a kernel, the entire magnetization state has to be copied to global memory, which has the lifetime of the host program, in between executions of the kernels. This copying data back and forth takes some time.

3.3 Optimization of GPU Based Magnetization Dynamics Simulator

The Monte Carlo simulations of magnetization dynamics properties require considerable computational resources and thus it is possible and desirable to further improve our computing performance by optimizing the kernel functions, memory access and block/grid configuration.

3.3.1 Optimize Instruction Usage

Some operations take a longer time to execute than other operations. For example, division using "/" is more costly than $fdividef()$, and they both cost much more than multiplication. Usually, a "/" operation takes 36 clock cycles and $fdividef()$ takes 20 clock cycles, whereas a multiplication takes only 4 clock cycles. In order to maximize the speed-up of the GPU, the use of slow operations should be minimized and, when possible, we should exchange them with fast operations[130].

This method can be applied to many steps within our calculations. For example, when determining the random time duration of magnetization precession without scattering in our simulation, we need to perform the calculation:

$$\tau = -\frac{1}{\Gamma}\ln[1 - P(\tau)]. \tag{3.1}$$

where P is a random number uniformly distributed between 0 and 1 and Γ is the total scattering rate. Instead of performing the division operation every time, it can be benefical to store $\Gamma_r = \frac{1}{\Gamma}$ instead of Γ in memory and perform a multiplication at each step:

$$\tau = -\Gamma_r \ln[1 - P(\tau)]. \tag{3.2}$$

In addition, since P is a random number uniformly distributed between 0 and 1, so also is $(1 - P)$. We could replace $(1 - P)$ with P so a minus opertation is not necessary each time we generate a random time duration of magnetization precession without scattering. Following is the equation we use:

$$\tau = -\Gamma_r \ln[P(\tau)]. \tag{3.3}$$

3.3.2 Optimize Memory Structure

On graphics cards, memory access is very costly compared to operations on registers. There are different memory spaces on the GPU and they each have different bandwidths. Thus, memory optimization is one of the most important considerations for performance. Global memory space is off-chip but is the only way to communicate data between the host CPU and device GPU. The amount of global memory is rather large and the global memory bandwidth is good. Memory access to global memory should be coalesced to achieve the best performance. Shared memory space is on-chip and, as a result, it is much faster than global memory. Shared memory latency is roughly 100 times lower than global memory latency, provided that there are no band conflicts between the threads[85]. Simulation should maximize

the memory access efficiency by using as much fast memory and as little slow-access memory as possible.

3.3.3 Maximize Computation Potential

In order to maximize the use of GPU computation resources, one has to maximize parallel execution by determining the optimal thread number per multiprocessor. Since the warp size is 32 threads, the best block size would be a multiple of 32. As a result the number of threads per block should always be a multiple of 32 and it is better if is 192 or more. The number of blocks should be a multiple of the number of multiprocessors on the GPU and the number of blocks that run simultaneously on each multiprocessor[85].

The number of blocks and warps that can reside and be processed together on the multiprocessor for a given kernel depends on the amount of registers and shared memory used by the kernel and available on the multiprocessor. If there are not enough registers or shared memory available per multiprocessor to process at least one block, the kernel will fail to launch.

To maximize the computation potential, our simulations assign 256 threads per block which is a multiple of 32 while having 42 blocks of threads which is a multiple of the number multiprocessors (there are 7 multiprocessors in a NVIDIA GTX 460 card). In this way, 10,752 separate realizations of random magnetization dynamics are simultaneously computed and they are very well mapped to the GPU structure.

3.4 Numerical Results

As all current CUDA-enabled devices are optimized for 32-bit floating point precision, this was the precision used in our code. The results from our 32-bit precision code have been compared to results from our MATLAB implementation performed in double precision and no significant difference is observed. This confirms that single-precision floating point calculations are sufficient.

To test the accuracy of GPU simulator, thermal relaxations of an uniaxial cobalt particle to the superparamagnetic state have been simulated. As shown in chapter two, in the superparamagnetic state the equilibrium distribution has a Boltzmann-type form. We compute the equilibrium distribution through Monte Carlo simulations and compare between the Boltzmann expression and our numerical simulations for different sets of anisotropy parameters. The agreement between Monte Carlo simulations and the Boltzmann formula is quite good.

The numerical results confirm that our GPU implementation of the Monte Carlo simulation can produce adequate results of the jump-noise driven Landau-Lifshitz equation under a much more acceptable calculation time.

3.5 Computational Cost and Performance Comparison

To compare CPU and GPU speed, the code developed for the CUDA implementation has been carefully converted to a CPU equivalent to perform exactly the same computations as the CUDA code, including the sequence of random number generator. The CPU equivalent program runs on a Intel Xeon processor at 2.13

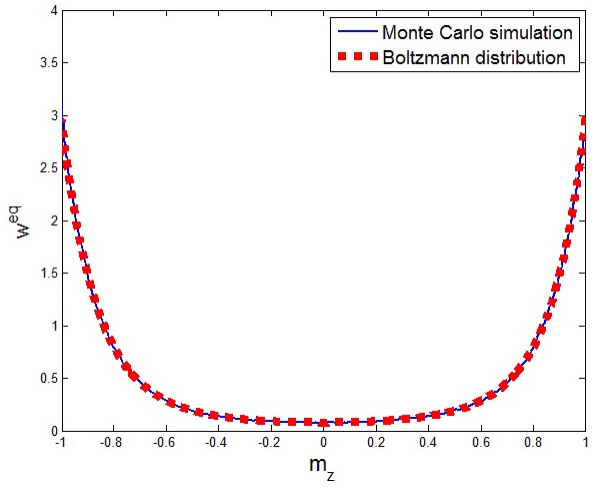

Figure 3.4: Equilibrium distribution in the superparamagnetic state of uniaxial cobalt nanoparticle (computations performed for the following parameters: $D_x = 0.2$ $D_y = 0.2$ $D_z = 0.01$ $M_s = 1.42 \times 10^6$ $\gamma = 1.837$ $T = 300$ $V = 2 \times 10^{-25}$ $\sigma = 0.1$ $B = 10^{12}$)

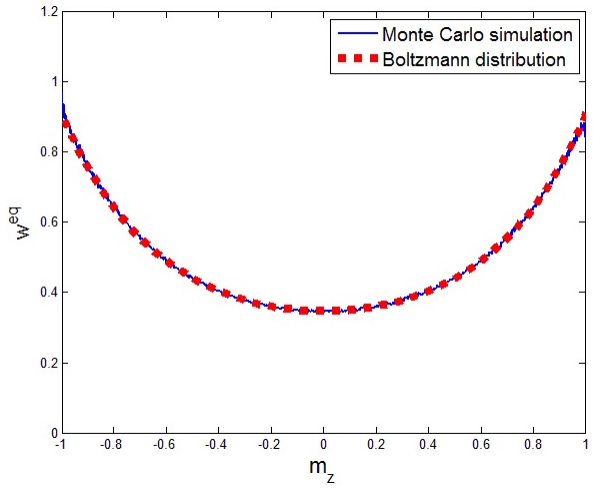

Figure 3.5: Equilibrium distribution in the superparamagnetic state of uniaxial cobalt nanoparticle (computations performed for the following parameters: $D_x = 0.35$ $D_y = 0.35$ $D_z = 0.3$ $M_s = 1.42 \times 10^6$ $\gamma = 1.837$ $T = 300$ $V = 2 \times 10^{-25}$ $\sigma = 0.1$ $B = 10^{12}$)

GHz with 48 GB RAM.

We can see from the above table that though the two implementations per-

Table 3.1: Performance Comparison

Number of realizations	CPU single-thread computation time (s)	GPU multi-thread computation time (s)	Speed-up factor
1792	43974.5	272.9	161.1
5376	132123.9	641.5	206.0
10752	263234.3	1211.9	217.2

form the same task using the same kernel function, a speed-up factor of more than 200 has been observed in GPU multi-thread implementation in comparison with the conventional CPU single-thread implementation when compute 10,752 separate Monte Carlo realizations. It is also clear from the table that the speed-up factor of GPU implementation over CPU implementation increases as the number of realizations calculated increases. This is because with a larger number of separate realizations, calculations are better mapped to the GPU structure so the processors are kept busy all the time and memory latency is very well hidden.

Chapter 4

Magnetization Dynamics at Low Temperatures and at Elevated Temperatures

In the previous chapters, we have demonstrated that the magnetization dynamics model with jump-noise process is more consistent with physical origin of damping and an efficient numerical technique for this model has been developed. In this chapter, the analysis framework of modeling the thermal fluctuations in magnetic systems using a jump-noise process is extended to study magnetization dynamics at a very wide range of temperatures.

Low temperature behavior of magnetization dynamics is of great scientific interest because the phenomenon of macroscopic tunneling of magnetization has been experimentally observed. Before any experiment was performed, it has been predicted theoretically[103, 104, 105, 106, 107] that macromagnetic quantum tunneling effect can be observed in magnetic systems. The macroscopic tunneling of magnetization is mostly studied by measuring the temperature dependence of magnetic relaxation. At high temperatures, magnetization reversal is caused by thermal fluctuations which drive the system above energy barrier created by magnetic anisotropy. This magnetization relaxation rate shows an exponential decay with respect to temperature decrease. When temperature is very low, thermal activation becomes extremely weak so magnetization relaxation should be really rare.

However, theoretical prediction suggests that there is still possibility to detect magnetization reversal. This reversal at low temperatures is because magnetization is able to tunnel through the energy barriers and this effect is called magnetic quantum tunneling[108, 109].

Modeling of high temperature behavior of magnetization dynamics is also of great scientific importance due to the recent advances in heat-assisted magnetic recording technology. In HAMR, temperature is raised locally using ultrafast pulsed laser so the coercivity of the magnetic storage medium at the bit is lowered and a realistically achievable magnetic write field can be used to write data to the medium. The classic Landau-Lifshitz or Landau-Lifshitz-Gilbert equation doesn't work for this case since it considers magnitude of magnetization as a constant and ignores longitudinal relaxation of the dynamics. The magnitude of magnetization is not conserved when temperature is close to the Curie temperature, thus a model is necessary for high temperature dynamics. A widely used model to describe magnetization dynamics at elevated temperature is the Landau-Lifshitz-Bloch equation[18, 53] which is derived from the Fokker-Planck equation and the derivation uses the mean-field approximation. Details of this equation have been discussed in chapter one. It is very desirable to develop one generalized equation without approximations. In this chapter we will extend our framework of modeling the thermal fluctuations in magnetic systems using a jump-noise process and will develop a generalized equation that conincides with the Landau-Lifshitz equation at low temperatures and is also valid up to and beyond the Curie temperature. The generalized equation has both longitudinal and transverse damping terms, and the mathematical form

of this equation is similar to the Landau-Lifshitz-Bloch equation. The longitudinal and transverse damping terms emerge directly from the structure of a jump-noise process which accounts for thermal interactions.

4.1 Random Switching of Magnetization

The mechanisms of the magnetization switching process have been widely discussed and have prompted intense research activities, motivated in particular by applications to magnetic data storage technology. Typically, at zero field, the energy barrier is very high so magnetization reversal is rarely observed. However, the energy barrier can be lowered by applying a magnetic field in the opposite direction of the magnetization. Here we are interested in the random switching process due to thermal excitations because of its important applications in thermal stability of magnetic recording devices. Long-term themal stability of magnetic storage devices is preferred, however, random and unstable distributions of magnetization directions are created by thermal fluctuations and long-term thermal switching would occurs due to the possibility of overcoming thermal energy barriers in the magnetic systems. Here we study particles whose magnetic moment has only two stable orientations. Even if these thermal fluctuations are small compared to the energy barrier, the magnetization will stay in a local energy minimum during many precessional periods with small jumps but it still has a certain probability to surmount the energy barrier separating the two energy minima and appear in the other minima. Typically when temperature fluctuations are small as compared to energy barriers, the

magnetization reversal happens due to thermal transitions through energy barriers. The probability of magnetization reversal is determined by the Arrhenius-Neel formula which is based on the Arrhenius equation proposed by Svante Arrhenius in 1889, Neel relaxation theory developed by Louis Neel in 1949[119] and Neel-Brown theory derived by Brown[14]. The Arrhenius-Neel law has the following form:

$$f = f_0 e^{-\frac{\Delta E}{k_B T}}. \tag{4.1}$$

where f_0 is a characteristic of the material called the attempt frequency which ranges from $10^9 Hz$ and $10^{11} Hz$ for magnetic systems, ΔE is the energy barrier, k_B is the Boltzmann constant, T is the temperature and their product is the thermal energy. We can see from the equation that the relaxation frequency is an exponential function of temperature, so the probability of magnetization reversal will increase exponentially with temperature increasing. Also, since the energy barrier is proportional to the grain volume, the flipping probability becomes rapidly negligible for large nanoparticles. The thermally activated magnetization reversal process has been the subject of much study recently[89, 90, 91, 92, 93, 94, 95, 96, 97].

As discussed above, a theory about quantum tunneling of magnetization has been developed that magnetization is able to tunnel through the energy barriers created by anisotropy [101, 102]. Researchers have also experimentally investigated this process and measurements have been performed at very low temperatures to test this hypothesis on a variety of materials such as BaFeCoTiO[110] Mn_{12}[108, 112, 111], Co[113], Ni[113, 114] and ferritin[115, 116, 117, 118]. These results show agreement with theoretical predictions. The figure 4.1 is taken from experimental

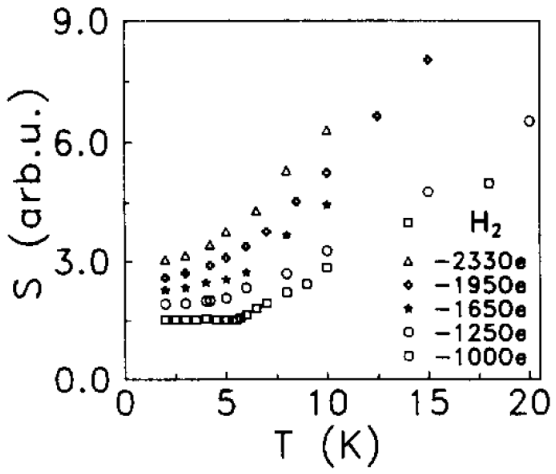

Figure 4.1: Experimental data of magnetic quantum tunneling[109]

study by Zhang *et al* in 1995. The curves show that at high temperatures the magnetization reversal of these particles follows the thermal activation theory while at lower temperature the reversal rate strongly deviates from it and confirms the predictions of the existence of magnetic quantum tunneling effect. There has been some research on modeling the low temperature thermally activated magnetization reversal processes in the micromagnetic framework [120, 121, 122, 123, 124]. These models involve quantum mechanical analysis of spin-bath interactions and spin-spin interactions.

The framework of modeling the thermal fluctuations as a jump-noise process can be extended to understand the long term dynamics of the magnetization reversal process. In this section, an approach to determine magnetization reversal probability is developed based on the jump-noise process driven magnetization dynamics model. We consider a system with two stable magnetization states that are parallel and antiparallel to the easy axis. Between these states there is an energy barrier due

to the anisotropy. This system is expected to escape from one state to the other either by thermal activation over the barrier at high temperatures or by quantum tunneling at low temperatures. As discussed in chapter one, the jump-noise process approach of magnetization dynamics under thermal effects leads to a integral-partial differential equation for transition probability density. In this section, we will show that this equation can be reduced to a Master equation using the Kramers-Brown quasi-local equilibrium approximation without any additional assumptions.

The numerical implementation of this approach will then be discussed and computational results of thermal switching of magnetization for a very wide range of temperatures will be presented. The computations confirm that there are two distinct regimes of magnetization switching and the regimes are controlled by the thermal bath through the parameters of the jump-noise process. The first regime occurs for sufficiently high temperatures. The temperature dependence of the magnetization switching rate coincides with that for thermally activated switching phenomena. The second regime occurs at very low temperatures. The magnetization switching rate exhibits some features that coincide with experimental results of macroscopic quantum tunneling effect of magnetization. What makes this approach different from the traditional approach to predict quantum tunneling effects is that, this two different temperature dependent regimes emerge directly from the properties of a jump-noise process and no quantum considerations are involved in our analysis.

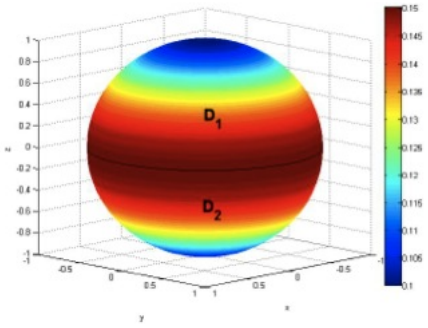

Figure 4.2: Energy distribution of an uniaxial particle

4.1.1 Mathematical Model

We study the random switching of magnetization in uniaxial nanoparticles with only two equilibrium (minimum energy) states located in the two wells D_1 and D_2 that completely cover Σ, i.e., $D_1 + D_2 = \Sigma$. The energy distribution is illustrated in Fig 4.2. More complicated energy landscapes can be treated in a similar way.

To study the random switching of magnetization, we will start with the Landau-Lifshitz magnetization dynamics driven by a jump-noise process described by equation (1.20). When the energy barrier between wells D_1 and D_2 is sufficiently large compared with kT , the noise-driven magnetization switching process occurs on a very slow time scale. In this case Kramers and Brown [19, 125] suggested that the switching is a quasi-stationary diffusion process. So at any moment we expect a Boltzmann distribution will have been established in an energy well a long time before an appreciable number of particles have switched due to thermal fluctuations. The Kramers-Brown quasi-local approximation for the transition probability density

function can be written as follows:

$$w(\mathbf{M},t) \simeq \sum_{i=1}^{2} P_i(t) w_{0i}(\mathbf{M}). \tag{4.2}$$

where $P_i(t)$ is the probability of $\mathbf{M} \in D_i$ at time t and it has the following Boltzmann form:

$$w_{0i}(\mathbf{M}) = \frac{\varphi_i(\mathbf{M})}{Z_i} e^{-\frac{g(\mathbf{M})-g_i}{kT}}. \tag{4.3}$$

In the last formula, $\varphi_i(\mathbf{M}) = 1$ for $\mathbf{M} \in D_i$ and $\varphi_i(\mathbf{M}) = 0$ for $\mathbf{M} \notin D_i$, g_i are energy minima and Z_i are the normalization constants such that the total probability that $\mathbf{M} \in D_i$ is one:

$$\int_{D_i} w_{0i}(\mathbf{M}) d\Sigma = 1. \tag{4.4}$$

The above normalization is consistent with the definition of $P_i(t)$ such that

$$P_i(t) = \int_{D_i} w(\mathbf{M},t) d\Sigma. \tag{4.5}$$

By using the Kramers-Brown approximation (4.2) without any additional assumptions, it can be shown [1] that the above equations can be transformed into the following Master equation:

$$\frac{dP_k}{dt} = \sum_{i=1}^{2} \lambda_{ki} P_i - P_k \sum_{i=1}^{2} \lambda_{ik}, (k = 1, 2), \tag{4.6}$$

where

$$\lambda_{ki} = \int_{D_k} \left(\int_{D_i} S(\mathbf{M}', \mathbf{M}) w_{0i}(\mathbf{M}') d\Sigma' \right) d\Sigma. \tag{4.7}$$

By substituting the expression for the transition probability rate (1.29) , the last expression can be written in the form

$$\lambda_{ki} = \frac{A}{Z_i} \int_{D_k} \left(\int_{D_i} e^{-\frac{|\mathbf{M}-\mathbf{M}'|^2}{2\sigma^2}} e^{-\frac{g(\mathbf{M})+g(\mathbf{M}')-2g_i}{2kT}} d\Sigma' \right) d\Sigma. \tag{4.8}$$

The Master equation can be further simplified into the following equation:

$$\frac{dP_1}{dt} = -\frac{dP_2}{dt} = -\lambda_{21}P_1 + \lambda_{12}P_2. \tag{4.9}$$

It is clear from (4.9) that under the condition of a high energy barrier and small thermal noise and given initial conditions, the evolution of the system under thermal fluctuation can now be determined by simply solving a set of deterministic first-order differential equations.

4.1.2 Numerical Results

Then magnetization switching is studied by using the Master equations (4.8) (4.9) with the following initial conditions

$$P_1(0) = 0, \qquad P_2(0) = 1, \tag{4.10}$$

which means the orientation of magnetization is initially in energy well 2 with probability 1.

Equations (4.9) can be easily solved analytically under the above initial conditions. The solutions should have the following form:

$$P_1(t) = \frac{\lambda_{12}}{\lambda_{12}+\lambda_{21}} - \frac{\lambda_{12}}{\lambda_{12}+\lambda_{21}} e^{-(\lambda_{12}+\lambda_{21})t}, \tag{4.11}$$

$$P_2(t) = \frac{\lambda_{21}}{\lambda_{12}+\lambda_{21}} + \frac{\lambda_{12}}{\lambda_{12}+\lambda_{21}} e^{-(\lambda_{12}+\lambda_{21})t}, \tag{4.12}$$

From the above expressions we can see that the evolution of magnetization reversal probability can be described by a single exponential function of time.

To illustrate the evolution of magnetization reversal probabilities, $P_1(t)$ has been computed for different values of applied field along the anisotropy axis. The

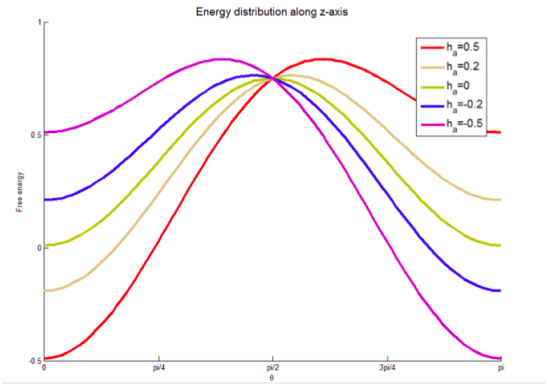

Figure 4.3: Distribution of normalized microscopic energy for different applied fields along the z-axis.

following expression is used to compute normalizaed microscopic energy g:

$$g(\theta) = -\frac{k_{\text{eff}}}{2}\cos^2\theta - h_a\cos\theta, \tag{4.13}$$

where g is the microscptic energy of the particle normalized by $\mu_0 M_s^2 V$, with V being the particle volume and h_a is the applied magnetic field normalized by magnitude of magnetization M_s. Since the energy distribution has rotational symmetry, we only plot the energy values along the z-axis. Figure 4.3 illustrate the energy distribution for different applied fields along the z-axis.

Figure 4.4 presents the computed plots of $P_1(t)$ for different values of applied magnetic field. The orientation of magnetization is initially in energy well 2 with probability 1, so at time 0 the value of $P_1(t)$ is always 0. It is apparent from this figure that for zero applied magnetic field, after a long enough time the magnetization will end up either in energy well 1 or enegy well 2 with a same probability so the $P_1(\infty) = 0.5$. When the applied magnetic field is not zero, the magnetization will tend to stay in the energy well with higher energy barrier, so $P_1(\infty)$ monotonically

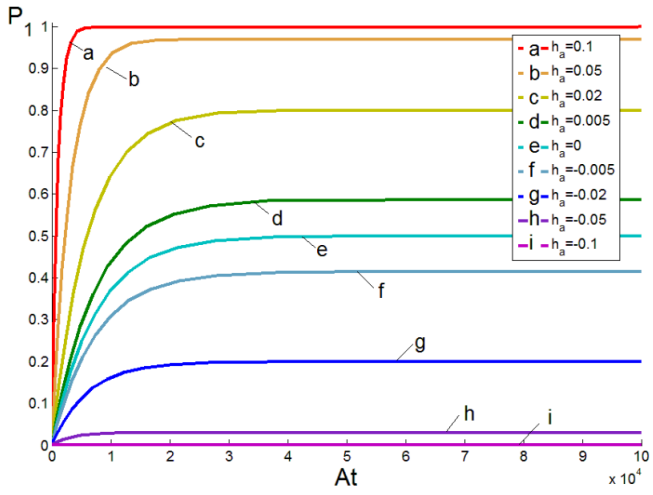

Figure 4.4: Evolution of magnetization reversal probability at 300 K for different applied fields along the z-axis.

increases with the monotonic increase in energy barrier height of energy well D_1 due to the applied field. It is also clear from this figure that as the energy barrier decreases, $P_1(t)$ increases faster.

To study the temperature dependence of magnetic switching properties, we have also numerically studied the initial switching rate as a function of temperature. From initial conditions, the following equations are true during the initial stage:

$$P_1(t) \simeq 0, \qquad P_2(t) \simeq 1. \tag{4.14}$$

Consequently, by substituting the initial conditions into equation (4.9) it can be derived that at initial stage, the switching rate can be identified as follows:

$$\frac{dP_1(t)}{dt} \simeq \lambda_{12}. \tag{4.15}$$

Since the initial switching rate equals to λ_{12}, properties of the initial switching rate can be identified by analyzing the mathematical structure of λ_{12}. It is clear from formula (4.8) that two distinct performance of the value λ_{12} may occur for

sufficient low and high temperatures, as a result, two different regimes of magnetization switching rate may be revealed. By evaluating the structure of λ_{12} we can see that for appreciably large T, the first exponential factor in the integrand of (4.8) dominates and the integrand is strongly peaked in the narrow region near the boundary between D_1 and D_2. In this narrow region, the second exponential factor of the integrand in (4.8) is close to $e^{-(g_{\max}-g_i)/kT}$. This is of the same mathematical form of the Arrhenius Law thus expected to lead to the classical thermally activated switching case of the switching rate. At very low temperatures, the second exponential factor in the integrand dominates and it is strongly peaked for $\mathbf{M}$ and $\mathbf{M}'$ around their respective energy minima. It is reasonable to expect that this structure will not follow the classical situation of thermally activated switching but lead to a different temperature dependence of switching rate at very low temperatures.

The above qualitative reasoning can be supported by numerical evaluation of the initial swithching rate λ_{12}. Since we are considering uniaxial nanoparticles with easy axis aligned with the direction of z-axis, the micromagnetic free energy distribution has rotational symmetry. The mathematical structure of the initial swithching rate λ_{12} can be better visualized by evaluting the following formula where magnetization is characterized using the θ value while the ϕ of a magnetization is ignored due to the rotational symmetry:

$$f_{12}(\theta,\theta') = \frac{A}{Z_2} e^{-\frac{g(\theta)+g(\theta')-2g_2}{2kT}} \int_0^{2\pi}\int_0^{2\pi} e^{-\frac{|\mathbf{M}(\theta,\phi)-\mathbf{M}(\theta',\phi')|^2}{2\sigma^2}} d\phi d\phi' \tag{4.16}$$

The computations are illustrated by Figure 4.5 where the $f_{12}(\theta,\theta')$ is plotted for different temperatures. It is apparent from Figure 4.5a that at $1K$, the function

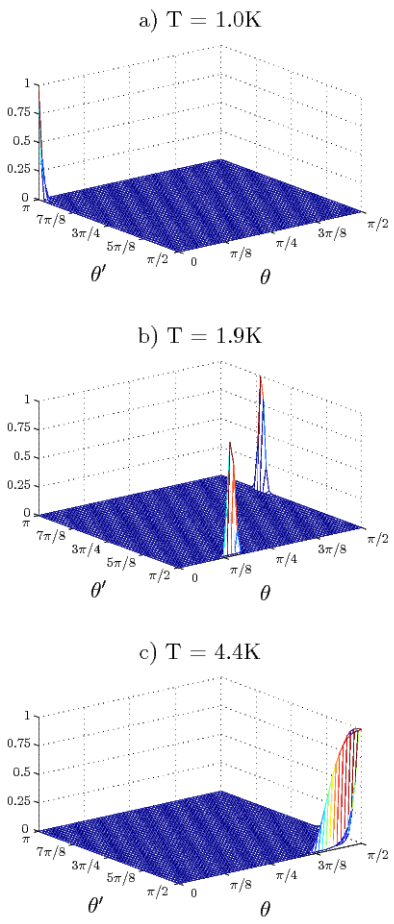

Figure 4.5: $f_{12}(\theta, \theta')$ at various temperatures.

$f_{12}(\theta, \theta')$ is strongly localized around the point ($\theta = 0$, $\theta' = \pi$) which corresponds to $\mathbf{M}$ and $\mathbf{M}'$ being at their respective minima. As the temperature is increased to 1.9 K, two strongly pronounced maxima of $f_{12}(\theta, \theta')$ abruptly appear along the lines $\theta = \pi/2$ and $\theta' = \pi/2$ as shown in Figure 4.5b. As the temperature is further increased, these two maxima of $f_{12}(\theta, \theta')$ move along the two lines and merge together at 4.4 K as shown in Figure 4.5c. At higher temperatures this localized maximum at the point ($\theta = \pi/2$, $\theta' = \pi/2$) continues to grow.

These two different localizations of the integrand in formula (4.16) result in

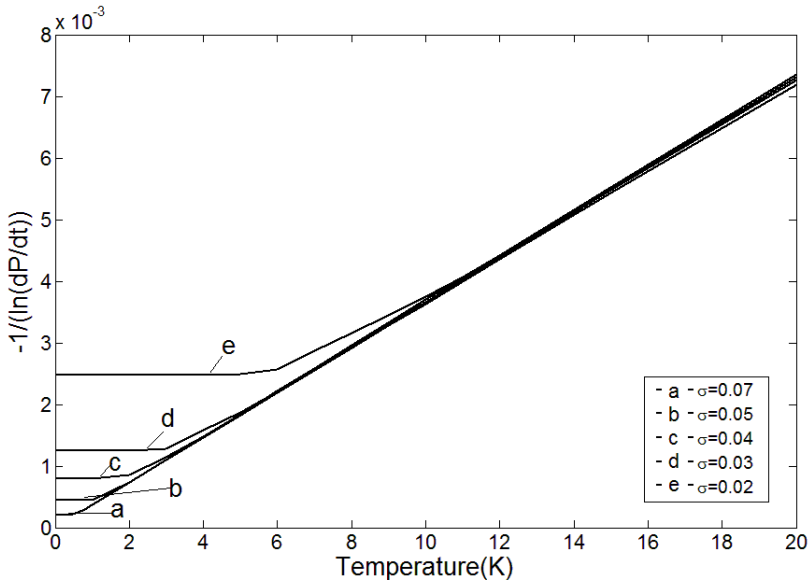

Figure 4.6: Temperature dependence of magnetization switching rate with different noise strength.

two different temperature dependences of magnetization switching rate. This is illustrated by Figure 4.6 where the quantity $-1/\ln\lambda_{12}$ is plotted versus temperature for different values of σ.

This figure clearly reveals the existence of two distinct regimes of magnetization switching. And the curves of switching rate coincide very well with those from experimental data shown in 4.1. The linear variation of $-1/\ln\lambda_{12}$ with respect to temperature at relatively high temperatures can be clearly identified with traditional thermally activated switching. That is, at high temperature the Arrhenius law is approximately followed. With decreasing temperature, the curves flatten out and becomes temperature independent. The flat part of the curves reveals that at very low temperature therelaxation from one state to another is enhanced above the thermally activated rate. These deviations from the simple model of thermally assisted

magnetization reversal are consistent with experimental observations of macroscopic quantum tunneling of magnetization at very low temperatures. It is also clear from the figure that the transition from the thermal regime to quantum regime is quite sharp. The crossover temperature occurs at a few Kelvins and depends on the value of σ. All of these properties of the switching rate are consistent with the theoretical predictions of magnetic quantum tunneling effect and experimental data. Since the tranditional theoretical explanation requires quantum mechanical analysis of spin-bath interactions and spin-spin interactions, it is remarkable that in our analysis the two regimes performance has emerged from the properties of a jump-noise process and that no quantum mechanical considerations have been involved.

4.2 Magnetization Dynamics at Elevated Temperatures

Modeling of high temperature behavior of magnetization dynamics is also of great importance due to the recent advances in heat-assisted magnetic recording technology[127] and all-optical magnetization switching[128]. In heat-assisted magnetic recording, temperature is raised locally above the Curie temperature using ultrafast pulsed laser so the coercivity of the magnetic storage medium at the bit is lowered and a realistically achievable magnetic write field can be used to write data to the medium. The classic magnetization dynamics model is not valid to model the elevated temperature dynamic performance. The classical Landau-Lifshitz and Landau-Lifshitz-Gilbert equations describe magnetization dynamics with the property that the magnitude of magnetization is conserved, i.e., magnetization is con-

sidered as a vector of fixed length and its longitudinal relaxation is ignored. This property is usually justified for well below the Curie temperature because at such temperatures the local exchange interaction prevails over all other forces at the smallest spatial scale and is compatible with the continuous media hypothesis of micromagnetics. However, this property may not be true at elevated temperatures. If we consider the changes of magnetization magnitude at elevated temperatures, the magnetization dynamics equation of a ferromagnet should contain both transverse and longitudinal relaxation terms. For this reason a model is necessary for high temperature dynamics. A widely used model to describe magnetization dynamics at elevated temperature is the Landau-Lifshitz-Bloch equation[18, 53]. It is a generalization of the classical Landau-Lifshitz equation while is applicable at both elevated temperatures and low temperatures so that magnetization dynamics can be described when the magnetization magnitude is not conserved. The Landau-Lifshitz-Bloch equation is derived from the Fokker-Planck equation and the derivation uses the mean-field approximation. It is very desirable to develop one such generalization without approximations and in this section such a generalized dynamic equation is developed. It is based on the same approach in chapter one which is to describe the thermal bath effects using a jump-noise process. The only difference is that previously, the magnetization dynamics is restricted to the sphere $|\mathbf{M}(t)| = Ms = const$ due to the microscopic constraint, but at elevated temperatures this constraint is no longer valid. The magnetization magnitude is allowed to change, and these changes are accounted for by relaxing this constraint on a jump-noise process and by introducing an additional term in the effective magnetic field

or the free magnetic energy [126].

4.2.1 Mathematical Model

Our model is based on the same approach in chapter one which is to describe the thermal bath effects using a jump-noise process. Consequently, we will start with the magnetization dynamics equation (1.20). There, the magnetization dynamics is studied at temperatures T well below the Curie temperature T_c so that the dynamics occurs only on the sphere Σ defined by the formula (1.21). This is achieved in chapter one by restricting the transition probability rate $S(\mathbf{M}(t), \mathbf{M}')$ to the sphere Σ. At elevated temperatures close to T_c there is no such restriction so $S(\mathbf{M}, \mathbf{M}')$ can be defined for any $\mathbf{M}$ and $\mathbf{M}'$. Since the magnetization magnitude is allowed to change, an additional term need to be introduced in the free magnetic energy to account for the changes of the magnetization magnitude.

$$g(\mathbf{M}) = g_0(\mathbf{M}) + \tilde{g}(M), \tag{4.17}$$

where $g_0(\mathbf{M})$ is the classical free micromagnetic energy traditionally used for magnetization dynamics on the sphere Σ, while $\tilde{g}(M)$ is the part of the free magnetic energy which is due to the deviation of the magnetization magnitude from M_s.

The effective magnetic field $\mathbf{H}_{\text{eff}}$ is related to $g(\mathbf{M})$ by the formula

$$\mathbf{H}_{\text{eff}} = -\frac{1}{\mu_0 V}\nabla g(\mathbf{M}). \tag{4.18}$$

This formula implies that at the equilibrium (energy minimum) state we have

$$\mathbf{H}_{\text{eff}} = 0. \tag{4.19}$$

This is quite different from the classical micromagnetic equilibrium condition expressed by the Brown equation

$$\mathbf{M} \times \mathbf{H}_{\text{eff}} = 0. \tag{4.20}$$

This difference is due to the fact that at elevated temperatures equilibrium states are found as a result of unconstrained minimization of $g(\mathbf{M})$, while in the classical micromagnetics equilibrium states are restricted to the sphere Σ.

In order to derive the damping parameter at elevated temperatures, we follow the method used in chapter one. Similarly, the damping term for magnetization can be shown as average effects caused by the jump process $\mathbf{T}_r(t)$. First, we decompose the jump-noise process into two distinct terms: the expected (average) value and fluctuation:

$$\mathbf{T}_r(t) = E[\mathbf{T}_r(t)] + \mathbf{T}_r^{(0)}(t), \tag{4.21}$$

By neglecting the fluctuation term $\mathbf{T}_r^{(0)}(t)$, the magnetization dynamics can be described using the following deterministic equation:

$$\frac{d\mathbf{M}}{dt} = -\gamma \left(\mathbf{M} \times \mathbf{H}_{\text{eff}}\right) + E[\mathbf{T}_r(t)]. \tag{4.22}$$

Then we need to find the expression for $E[\mathbf{T}_r(t)]$ to fully describe the magnetization. Similar to (1.34), the expected value can be written as a integral equation. A slight difference here is that value need to be integrated over the whole space because at elevated temperatures the magnetization magnitude is no longer constraint to the sphere and $\mathbf{M}$ and $\mathbf{M}'$ can take any value in the whole space. For this reason,

the expected value of the jump-noise process can be written as follows:

$$E[\mathbf{T}_r(t)] = \iiint \mathbf{m} S(\mathbf{M}, \mathbf{M}+\mathbf{m}) d\mathbf{m}. \tag{4.23}$$

To evaluate the integral, we rewrite the expression in the follwing form by taking into account that $\mathbf{M} - \mathbf{M}' = \mathbf{m}$ and $g(\mathbf{M}) - g(\mathbf{M}') \simeq -\mathbf{m} \cdot \nabla g$

$$S(\mathbf{M}, \mathbf{M}+\mathbf{m}) \simeq A \exp\left\{ -\frac{|\mathbf{m}^2|}{2\sigma^2} - \frac{\mathbf{m} \cdot \nabla g}{2kT} \right\}, \tag{4.24}$$

which can be further transformed as follows:

$$\begin{aligned} S(\mathbf{M}, \mathbf{M}+\mathbf{m}) = A \exp & \left\{ \frac{1}{2} \left(\frac{\sigma |\nabla g|}{2kT} \right)^2 \right\} \\ & \times \exp \left\{ -\frac{1}{2\sigma^2} \left| \mathbf{m} + \frac{\sigma^2}{2kT} \nabla g \right|^2 \right\}. \end{aligned} \tag{4.25}$$

By substituting the last formula into equation (4.23), we find

$$E[\mathbf{T}_r(t)] = A \exp \left\{ \frac{1}{2} \left(\frac{\sigma |\nabla g|}{2kT} \right)^2 \right\} I, \tag{4.26}$$

where I is the notation for the following Gaussian integral

$$I = \iiint \mathbf{m} \exp \left\{ -\frac{1}{2\sigma^2} \left| \mathbf{m} + \frac{\sigma^2}{2kT} \nabla g \right|^2 \right\} d\mathbf{m}, \tag{4.27}$$

which can be evaluated as follows:

$$I = -\left(\sigma \sqrt{2\pi} \right)^3 \frac{\sigma^2 \nabla g}{2kT}. \tag{4.28}$$

Then we apply a similar technique to find the expression for the scattering rate $\lambda(\mathbf{M})$. Since $\lambda(\mathbf{M})$ can be written as a integral of $S(\mathbf{M}, \mathbf{M}')$:

$$\lambda(\mathbf{M}) = \iiint S(\mathbf{M}, \mathbf{M}') \, d\mathbf{M}', \tag{4.29}$$

we derive that

$$\lambda(\mathbf{M}) = A\left(\sigma\sqrt{2\pi}\right)^3 \exp\left\{\frac{1}{2}\left(\frac{\sigma|\nabla g|}{2kT}\right)^2\right\}. \tag{4.30}$$

By combining the above equations, we obtain

$$E[\mathbf{T}_r(t)] = \frac{\sigma^2}{2kT}\lambda(\mathbf{M})\mathbf{H}_{\text{eff}}, \tag{4.31}$$

and the magnetization dynamics equation at elevated temperatures becomes

$$\frac{d\mathbf{M}}{dt} = -\gamma\left(\mathbf{M}\times\mathbf{H}_{\text{eff}}\right) + \frac{\sigma^2}{2kT}\lambda(\mathbf{M})\mathbf{H}_{\text{eff}}. \tag{4.32}$$

The last equation suggests that average thermal relaxations of magnetization to the equilibrium (energy minimum) state occur along the direction of steepest energy decrease.

Since $\mathbf{M}$, $\mathbf{M}\times\mathbf{H}_{\text{eff}}$ and $\mathbf{M}\times(\mathbf{M}\times\mathbf{H}_{\text{eff}})$ are mutually orthogonal, any vector can be expresses using these three basis vectors. Because $\mathbf{H}_{\text{eff}}$ is orthogonal to $\mathbf{M}\times\mathbf{H}_{\text{eff}}$, the average value of the jumps $E[\mathbf{T}_r(t)]$ can be decomposed into the following form:

$$E[\mathbf{T}_r(t)] = -\alpha\mathbf{M}\times(\mathbf{M}\times\mathbf{H}_{\text{eff}}) - \nu\mathbf{M}. \tag{4.33}$$

By using the vector-algebra identity for a double cross product, the decomposition can also be written in the following form:

$$E[\mathbf{T}_r(t)] = \alpha|\mathbf{M}|^2\mathbf{H}_{\text{eff}} - \left[\alpha\left(\mathbf{M}\cdot\mathbf{H}_{\text{eff}}\right) + \nu\right]\mathbf{M}. \tag{4.34}$$

By comparing the above equation and equation (4.31), we can derive the following expressions for the transverse damping constant α and the longitudinal

damping constant ν:

$$\alpha = \frac{\sigma^2}{2kT|\mathbf{M}|^2}\lambda(\mathbf{M}), \tag{4.35}$$

$$\nu = -\frac{\sigma^2(\mathbf{M}\cdot\mathbf{H}_{\text{eff}})}{2kT|\mathbf{M}|^2}\lambda(\mathbf{M}). \tag{4.36}$$

Finally, by substituting formula (4.33) into equation (4.22), the following equation for magnetization dynamics at elevated temperatures can be derived:

$$\frac{d\mathbf{M}}{dt} = -\gamma(\mathbf{M}\times\mathbf{H}_{\text{eff}}) - \alpha(\mathbf{M}\times(\mathbf{M}\times\mathbf{H}_{\text{eff}})) - \nu\mathbf{M}. \tag{4.37}$$

This equation has a generalized form which contains both longitudinal and transverse damping terms. The corresponding damping parameters α and ν are given by formulas (4.35) and (4.36), respectively, and they depend on the magnetization and parameters of the jump-noise process. It is clear that the mathematical structure of this equation is similar to the structure of the Landau-Lifshitz-Bloch equation mentioned in chapter one. The difference is that our derivation of this equation is based on an entirely different conceptual basis. It is appreciably simpler and more physically transparent than in [18]. The longitudinal and transverse damping terms emerge in the presented derivation directly from the structure of a jump-noise process, while in [18], the Landau-Lifshitz damping term is introduced in the initial equation independently of the stochastic white-noise term.

4.2.2 Discussion

It is of great interest to further discuss the structure of the damping motion described using (4.37). Since $\tilde{g}(M)$ is the part of free energy that is due to the deviation of the magnetization magnitude from M_s, we can assume that $\tilde{g}(M)$ depends

only on the magnitude M of magnetization $\mathbf{M}(t)$ and it reaches its minimum on the sphere. This implies that the component $\tilde{g}(M)$ of free magnetic energy can be interpreted as an "energy penalty" caused by deviation of $|\mathbf{M}(t)|$ from M_s.

With the above assumption and by using formulas (4.17) and (4.18), we find

$$\mathbf{H}_{\text{eff}} = -\frac{1}{\mu_0 V}[\nabla_{\mathbf{M}} g_0(\mathbf{M}) - \tilde{g}'(M)\frac{\mathbf{M}}{M}], \tag{4.38}$$

where $\tilde{g}'$ is the derivative of $\tilde{g}$.

By substituting the last formula into the expression (4.36), we get

$$\nu = \frac{\sigma^2 \lambda(\mathbf{M})}{2kTM}\left(\mathbf{M} \cdot \nabla_{\mathbf{M}} g_0(\mathbf{M}) + \tilde{g}'(M)\right). \tag{4.39}$$

One way of choosing $\tilde{g}(M)$ is to use the Landau theory of second-order phase transition. According to this theory[129], near the Curie temperature T_c the function $\tilde{g}(M)$ can be represented as follows:

$$\tilde{g}(M) = -A_1(T_c - T)M^2 + A_2 M^4, \quad (A_1 > 0,\ A_2 > 0). \tag{4.40}$$

From the last formula we find

$$\tilde{g}'(M) = -2A_1(T_c - T)M + 4A_2 M^3, \tag{4.41}$$

and $\tilde{g}(M)$ achieves its minimum at

$$M_s(T) = \left(\frac{A_1(T_c - T)}{2A_2}\right)^{\frac{1}{2}}. \tag{4.42}$$

By using the last formula, the expression for $\tilde{g}(M)$ can be represented by the equation

$$\tilde{g}(M) = \frac{A_1^2}{4A_2}(T_c - T)^2 \left[\left(\frac{M}{M_s}\right)^2 - 1\right]^2. \tag{4.43}$$

From formulas (4.41) and (4.43) we can see that when temperature goes down, a very steep energy well is formed around the sphere Σ. This may cause the very fast relaxation dynamics of magnetization towards the sphere Σ. As a result of these relaxations, the subsequent magnetization dynamics will occur on the sphere Σ where $\nu = 0$ and the generalized dynamics equation (4.37) is reduced to the jump-noise process driven Landau-Lifshitz equation for low temperatures with α defined by formula (4.35).

Chapter 5

Conclusion and Outlook

In this dissertation, a jump-noise process driven Landau-Lifshitz equation has been numerically implemented to model random magnetization dynamics with thermal bath interactions. Magnetization phenomena have been investigated using this approach for a very wide range of temperatures and these phenomena can be connected with various technological applications. The primary strength of the jump-noise process driven magnetization dynamics approach over the traditional approach where the thermal fluctuations are accounted for by a white-noise process, is that the jump-noise term itself can describe the thermal effects in a magnetic system including both damping motion and fluctuations. The classical Landau-Lifshitz and Landau-Lifshitz-Gilbert damping terms can be derived as average effects caused by the jump-noise process. It has been demonstrated that this approach is clearly consistent with the physical origin of damping and scattering processes since both damping and fluctuation effects emerge from the jump-noise process. Numerical implementation has been developed for this approach and the numerical results comfirms the correctness of the analytical derivations. Numerical techniques implemented in the simulation are unconditionally stable. They preserve micromagnetic constraints and appreciably simplify the random component of Monte Carlo simulations. The accuracy and efficiency of the numerical techniques are demonstrated by

examples of Monte Carlo simulations that show an perfect agreement between the equilibrium distribution in the superparamagnetic state and a Boltzmann-type distribution. To speed up the Monte Carlo simulations of magnetization dynamics, a parallel algorithm is developed on GPUs. The simulation tasks are perfectly mapped to the GPU architecture and a speed-up factor of about 200 is observed in GPU Monte Carlo simulations in comparison with the traditional single-threaded CPU simulations. Several magnetization dynamics properties have been investigated using this analysis framework. In particular, magnetization switching processes are investigated for a very wide range of temperatures. By using a Kramers-Brown quasi-local equilibrium approximation, a Master equation is derived for magnetization random switching when the energy barrier between energy wells is sufficiently large in comparison with the thermal energy. The Master equation is a first-order differential equation so that the evolution of reversal probabilities can be easily solved using the Master equation without any randomness. Numerical implementation of the Master equation shows consistency with experimental data where the high temperature switching agrees with the Arrhenius law of thermal activation while the low temperature switching has many features traditionally attributed to the phenomena of macroscopic magnetization tunneling. In addition, a generalized stochastic equation is developed to describe the magnetization dynamics at elevated temperatures. Such a generalization is derived based on the same approach of describing the thermal bath effects by a jump-noise process, and the generalized equation conincides with the Landau-Lifshitz equation at low temperatures and is also valid up to the Curie temperature. This equation has both longitudinal and

transverse damping terms, and the mathematical form of this equation is similar to that of the Landau-Lifshitz-Bloch equation. The difference is that the generalized equation we derived is based on a different conceptual basis and the longitudinal and transverse damping terms emerge directly from the structure of a jump-noise process which accounts for thermal interactions. There are several areas where the jump-noise process approach can be applied and incremental improvements can be made. The following are some of the improvements and topics that can be done in the future.

The numerical implementation of the jump-noise process driven magnetization dynamics approach can be extended by developing a finite element method with mid-point time-stepping and self-scattering scheme. This extended implementation would allow simulation of magnetization dynamic processes of magnetic bodies in arbitrary shape. For instance, the dynamic processes of a thin-film material in hard disk drives or a multi-layer structure in spin valves can be calculated in this way. In addition, the jump-noise process has two distinct parameters that characterized the noise. Their physical meanings should be further investigated to understand the relation of damping motion and thermal interactions. Moreover, in chapter four the thermally activated magnetization reversal process has been investigated using the jump-noise process driven approach. A deterministic Master equation is derived using only one assumption, the Kramers-Brown approximation. In order to find the applicability for the Master equation, the condition of the Kramers-Brown approximation should be very well understood. This approximation holds only when energy barriers created by anisotropy are sufficiently high in comparison with thermal ef-

fect. It is of great importance to identify the "sufficiently high" condition using a quantitative number. Future work in the jump-noise process driven dynamics framework could also be made by developing techniques to describe magnetization dynamics of a magnetic system in the presence of spin polarized current injection. Spintronics is a new area rising from nanomagnetism and there are numerous spintronic dynamic phenomena worth investigating and modeling. Finally, an averaging technique can be used to develop a slow time scale dynamic equation by using the magnetic free energy as a state variable. The stochastic dynamic equation of energy can also be used to analyze thermally activated magnetization reversal processes. And it can be used to identify the condition of the Kramers-Brown approximation and the limit of applicability of the Master equation. This direction can be pursued in future activities.

Bibliography

[1] I.Mayergoyz, G. Bertotti and C. Serpico, Phys. Rev. B 83, 020402 (2011).

[2] I.Mayergoyz, G. Bertotti and C. Serpico, J. Appl. Phys. 109, 07D312 (2011).

[3] I.Mayergoyz, G. Bertotti and C. Serpico, J. Appl. Phys. 109, 07D327 (2011).

[4] B. D. Cullity and C. D. Graham, *Introduction to Magnetic Materials*, Wiley (2009).

[5] Toshiba: Press Releases on Dec 14, 2004.

[6] P. Patel, IEEE Spectrum Mar 29, 2009.

[7] D. Houssameddine, U. Ebels, B. Delaet, B. Rodmacq, I. Firastrau, F. Ponthenier and M. Brunet, Nature materials 6, 447 (2007).

[8] Q. A. Pankhurst, J. Connolly, S. K. Jones and J. Dobson, J. Phys. D 36, R167 (2003).

[9] F.G. Snchez, *Modeling of field and thermal magnetization reversal in nanostructured magnetic materials*, Doctoral Dissertation, Universidad Autnoma de Madrid (2007).

[10] L.D. Landau and E.M. Lifshitz, Physik. Zeits. Sowjetunion, 8, 153 (1935).

[11] W.F. Brown Jr, Phys. Rev. 58, 736 (1940).

[12] W.F. Brown Jr, J. Appl. Phys. 11, 160 (1940).

[13] W.F. Brown Jr,Phys. Rev. 54, 279 (1938).

[14] W.F. Brown Jr,*Micromagnetics*, Wiley (1963).

[15] J. Fidler and T. Schrefl, Appl. Phys. 33(2000).

[16] T.L. Gilbert, Phys. Rev. 100, 1245 (1955).

[17] T.L. Gilbert, IEEE Trans. Magn., 40, 3443 (2004).

[18] D.A. Garanin, Phys. Rev. B 55, 3050 (1997).

[19] W.F. Brown Jr, Phys. Rev. 130, 1677 (1963).

[20] A. Lee, Z. Liu, C. Serpico, G. Bertotti and I. Mayergoyz, J. Appl. Phys. 111, 07D115 (2012).

[21] Z. Liu, A. Lee, P. McAvoy, G. Bertotti, C. Serpico and I. Mayergoyz, IEEE Trans. Magn, 49, 3133 (2013).

[22] J. Tejada, X. X. Zhang, and E. M. Chudnovsky, Phys. Rev. B 47, 14977 (1993).

[23] J. Tejada, X. X. Zhang, and L. Balcells, J. Appl. Phys. 73, 6709 (1993).

[24] W. Wernsdorfer, E. Bonet Orozco, K. Hasselbach, A. Benoit, D. Mailly, O. Kubo, H. Nakano, and B. Barbara, Phys. Rev. Lett. 79, 4014 (1997).

[25] Z. Liu, A. Lee, G. Bertotti, C. Serpico, and I. Mayergoyz, J. Appl. Phys. 111, 07D108 (2012).

[26] I. Mayergoyz, G. Bertotti, C. Serpico, Z. Liu, and A. Lee, J. Appl. Phys. 111, 07D501 (2012).

[27] G. Bertotti, I. Mayergoyz and C. Serpico, *Nonlinear Magnetization Dynamics in Nanosystems*, Elsevier (2009).

[28] D.V. Berkov, *Magnetization Dynamics Including Thermal Fluctuations: Basic Phenomenology, Fast Remagnetization Processes and Transitions Over High-energy Barriers*, Wiley (2007).

[29] A. Visintin, Japan J. Appl. Math.2, 69 (1985).

[30] G.Boling and S. Fengqiu, J. Math. Anal. Appl. 211, 326 (1987).

[31] J. Zhai, SIAM J. Math Anal. 30, 833(1999).

[32] X. Wu, *Two dimensional Landau-Lifshitz equations in micromagnetism*, Phd thesis, NewYork University (2000).

[33] S. Gustafson and J. Shatah, Comm. Pure Appl. Math. 55, 1136(2002).

[34] G.Garbou and P.Fabrie, Differential Integral Equations 14, 213(2001).

[35] G.Garbou and P.Fabrie, Comm. Appl. Anal. 5, 17 (2001).

[36] Y. Chen, Nonlinear Analysis 48, 411(2002).

[37] C. Melcher, Comm. Partial Differential Equations 30, 567(2005).

[38] C.J. Garcia-Cervera and X.P.Wang, Disc. Cont. Dyn. Sys. B 7, 87 (2005).

[39] P. Horley, V. Vieira, J. Gonzalez-Hernandez, V. Dugaev and J. Barnas, *Numerical Simulations of Physical and Engineering Processes*, chapter 6: Numerical Simulations of Nano-Scale Magnetization Dynamics, available from: http://www.intechopen.com/books/numerical-simulations-of-physical-and-engineering-processes/numerical-simulations-of-nano-scale-magnetization-dynamics.

[40] R. Ferre, Comput. Phys. Comm. 105, 169 (1997).

[41] L. Greengard and V. Rokhlin, *The rapid evaluation of potential fields in three-dimensions in Vortex methods*, Lecture Notes in Mathematics, vol. 1360, Berlin: Springer-Verlag, 1988.

[42] D. R. Fredkin and T. R. Koehler, IEEE Trans. Magn. 26, 415 (1990).

[43] D. Newns, W. Donath, G. Martyna, M. Schabes and B. Lengfield, J. Appl. Phys. 95, 3175 (2004).

[44] E. T. Ong, K. M. Lim, K. H. Lee and H. P. Lee, J. Comput. Phys. 192, 244 (2003).

[45] H. H. Long, E.T. Ong, Z. J. Liu and E. P. Li, IEEE Trans. Magn. 42, 295 (2006).

[46] User's Guide, National Institute of Standards and Technology, Gaithersburg, MD (2012).

[47] http://math.nist.gov/oommf

[48] http://www.magpar.net

[49] http://nmag.soton.ac.uk/nmag

[50] http://mumax.github.io

[51] A. Vansteenkiste and B. Van de Wiele, J. Magn, and Magn, Mate. 323, 2585 (2011).

[52] F Bloch, Physical Review 70, 460-473 (1946)

[53] D.A. Garanin, Physica A 172, 470 (1991).

[54] J.G. Zhu and H. Li, IEEE Trans. Magn. 49(2), 765772 (2013).

[55] T. W. McDaniel, J. Appl. Phys. 112, 013914 (2012).

[56] U. Kilic, G. Finocchio, T. Hauet, S. H. Florez, G. Aktas, and O. Ozatay, Appl. Phys. Lett. 101, 252407 (2012).

[57] C. Bunce et al., Phys. Rev. B 81, 174428 (2010).

[58] U. Atxitia, O. Chubykalo-Fesenko, J. Walowski, A. Mann, and M. Mnzenberg, Phys. Rev. B 81, 174401 (2010).

[59] O. Chubykalo-Fesenko, U. Nowak, R. W. Chantrell, and D. A. Garanin, Phys. Rev. B 74, 094436 (2006).

[60] D. R. Fredkin, Physica B 306, 26 (2001).

[61] W.Scholz , *Scalable parallel micromagnetic solvers for magnetic nanostructures*, Ph.D. thesis, Fakultat fur Naturwissenschaften und Informatik, Technische Universitat Wien (2003).

[62] W. Scholz, J. Fidler, T. Schrefl, D. Sub, R. Dittrich, H. Forster and B. Tsiantos, Comp. Mater. Scie. 28, 366 (2003).

[63] C.O.Mahany, *The Numerical Analysis of Stochastic Differential Equations*, available from: http://citeseerx.ist.psu.edu/viewdoc/download?doi=10.1.1.117.8043rep=rep1type=pdf.

[64] K. Burrage, P.M. Burrage and T. Tian, Proc. Royal Society 460, 373(2004).

[65] R. Kubo, Rep. Prog. Phys., 29 255 (1966).

[66] C. Serpico, I. Mayergoyz, and G. Bertotti, J. Appl. Phys. 89, 6991 (2001).

[67] M. Lundstrom, *Fundamentals of Carrier Transport (Vol. X of Modular Series on Solid State Devices)*, Addison-Wesley (1990).

[68] C. Jacoboni and L. Reggiani, Rev. Mode. Phys. 55, 645(1983).

[69] H.D. Rees, Phys. Lett A 26, 416 (1968).

[70] H.D. Rees, J. Phys. Chem. Solids 30, 643 (1969).

[71] M.H. Kalos, and P.A. Whitlock., *Monte Carlo methods, volume I: Basics"*, Wiley (1986).

[72] L. Devroye, *Non-Uniform Random Variate Generation*, Springer-Verlag (1986).

[73] L. Lopez-Diaz, D. Aurelio, L. Torres, E. Martinez, M. A. Hernandez-Lopez, J. Gomez, O. Alejos, M. Carpentieri, G. Finocchio, and G. Consolo, J. Phys. D 45, 323001 (2012).

[74] M. J. Flynn, IEEE Trans. Comput. C 21, 948 (1972).

[75] B. Block, P. Virnau and T. Preis, Comp. Phys. Comm. 181, 1549 (2010).

[76] E. Alerstam, T. Svensson, S. Andersson-Engels, J. Biomed. Opt. 0001;13(6):060504(2008).

[77] E.B. Ford, New Astronomy 14, 406 (2009).

[78] F. Molnar, T. Szakaly, R. Meszaros and I. Lagzi, Comp. Phys. Comm. 181, 105 (2010).

[79] T. Preis, P. Virnau, W. Paul and J.J. Schneider, New J. of Phys. 11, 093024 (2009).

[80] X. Gu, D. Choi, C. Men, H. Pan, A. Majumdar and S. Jiang, Phys. Medicine Biology 54, 6287 (2009).

[81] D. Gross, U. Heil, R. Schulze, E. Schomer and U. Schwanecke, SIAM J. Scientific Computing 31,4204 (2009).

[82] J.A. Anderson, C.D. Lorenz and A. Travesset, J. Comp. Phys. 227, 5342 (2008).

[83] I.S. Ufimtsev and T.J. Martinez, J. Chem. Theo. Comp. 4, 222 (2009).

[84] Nvidia CUDA C Programming Guide 4.0, Nvidia (2011).

[85] Nvidia CUDA best practices guide 4.1, Nvidia (2012).

[86] M. Matsumoto and T. Nishimura, ACM Trans. Modeling and Computer Simulation 8, 3 (1998).

[87] D. Knuth, *The Art of Computer Programming, Volume 2: Seminumerical Algorithms*, Addison-Wesley (1969).

[88] B.A. Wichmann and I.D. Hill, Comp. Stat. and Data Anal. 51, 1614(2006).

[89] X. Wang, H. N. Bertram and V.L. Safonov, J. Appl. Phys., 92(4) 2064 (2002).

[90] W. Ren, *Numerical methods for the study of energy landscapes and rare events*, PhD thesis, Conrant Institute of Mathematical Science, New York University (2002).

[91] W. E, W. Ren and E. Vanden-Eijnden, Phys. Rev. B 66, 2301(2002).

[92] W. E, W. Ren and E. Vanden-Eijnden, J. Appl. Phys. 93, 2275 (2003).

[93] W. Ren, Comm. Math. Sci 1,2377 (2003).

[94] W. E, W. Ren and E. Vanden-Eijnden, Comm. Pure Appl. Math (2004).

[95] D. Liu, *Topics in the analysis and computation of stochastic differential equations*, PhD thesis, Program in applied and computational mathematics, Princeton University (2003).

[96] D. Liu and C.J. Garcia-Cervera, J. Appl. Phys 98, 023903(2005)

[97] M.G. Reznikoff, *Rare events in finite and infinite dimensions*, PhD thesis, Conrant Institute of Mathematical Science, New York University (2004).

[98] S. Blundell,*Magnetism in Condensed Matter*, Oxford University Press (2001).

[99] D. Kannan, *An Introduction to Stochastic Processes*, North-Holland (1979).

[100] I.I. Gihman and A.V. Skorohod, *Stochastic Differential Equations*, Springer-Verlag (1972).

[101] E. M. Chudnovsky and L. Gunther, Phys. Rev. B 37, 9455 (1988).

[102] L. Thomas, F. Lionti, R. Ballou, D. Gatteschi, R. Sessoli, and B. Barbara, Nature 383, 145 (1996).

[103] J.L. van Hemmen adn A. Suto, Europhys. Lett. 1,481 (1986).

[104] E.M. Chudnovsky and L.Gunther, Phys. Rev. Lett. 60, 661 (1988).

[105] B.Barbara and E.M Chudonovsky, Phys. Lett. A145,205(1990).

[106] E.M Chudonovsky, O.Iglesias and P.C.Stamp, Phys.Rev.B 46,5392(1992).

[107] P.C.Stamp, Phys. Rev. Lett. 66,2802(1991).

[108] B.Barbara, J. Magn. Mater. 140-144, 1825(1995).

[109] J. Tejada and X. Zhang, J. Magn. Mater. 140-144, 1815(1995)

[110] W.Wernsdorfer, E.Bonet Orozco, K. Hasselbach, A.Benoit, D. Mailly, O.Kubo, H. Nakano and B.Barbara, Phys. Rev. Lett. 79, 20(1997).

[111] L.Thomas, F.Lionti, R.Ballou, D.Gatteschi, R.Sessoli and B.Barbara, Nature 383,145 (1996).

[112] C. Paulsen and J.G. Park, NATO ASI Series E: Applied Sciences 301, 189 (1995).

[113] W. Wernsdorfer, K. Hasselbach, D. Mailly, B. Barbara, A. Benoit, L. Thomas, G. Suran, Jour. Magn. Magn. Mater. 145, 12, 33(1995).

[114] N. Giordano and K. Hong, NATO ASI Series E: Applied Sciences 301, 257 (1995).

[115] D.D. Awschalom, J.F. Smyth, G. Grinstein, D.P. Di Vincenzo and D. Loss, Phys. Rev. Lett. 68, 3092 (1992).

[116] S. Gider, D. D. Awschalom, T. Douglas, S. Mann and M. Chaparala, Science 268, 77 (1995).

[117] J. Tejada, Science 272, 424 (1996).

[118] A. Garg, Science 272, 425 (1996).

[119] L.Neel, Ann. Geophys. 5, 99(1949).

[120] E.D. Boerner and H.N. Bertram, IEEE Trans. Magn. 33, 3052 (1997).

[121] R.W. Chantrell, J.D. Hannay, M. Wongsam, T. Schrefl and H.J. Richter, IEEE Trans. Magn. 34, 1839 (1998).

[122] A. Lyberatos, D.V. Berkov and R.W. Chantrell, J. Phys. Condens. Matter 5, 8911 (1993).

[123] Y. Nakatani, Y. Uesaka, N. Hayashi and H. Fukushima H, J. Magn. Magn. Mater. 168, 347 (1997).

[124] K. Zhang and D.R. Fredkin, J. Appl. Phys. 85, 5208 (1999).

[125] H. A. Kramers, Physica 7, 284 (1940).

[126] O.Chubykalo-Fesenko, U. Nowak, R. W. Chantrell and D. Garanin, Phys. Rev. B 74 (2006).

[127] Z. Zhang and I. D. Mayergoyz, J. Appl. Phys. 103, 07F510 (2008).

[128] C. D. Stanciu, F. Hausteen, A. V. Kimel, A. Kirilyuk, A. Tsukamoto, A. Itoh, and T. Rasing, Phys. Rev. Lett. 99, 047601 (2007).

[129] L.D. Landau., Zh. Eksp. Teor. Fiz. 7, 19 (1937).

[130] E. Alerstam, T. Svensson, and S. Andersson-Engels, J. Biomedical Optics Lett. 13, 060504 (2008).